NACA RM L50A04a

RESEARCH MEMORANDUM

MAXIMUM-LIFT CHARACTERISTICS OF A WING WITH THE LEADING-EDGE SWEEPBACK DECREASING FROM 45° AT THE ROOT TO 20° AT THE TIP AT REYNOLDS NUMBERS FROM 2.4×10^6 TO 6.0×10^6

By Roy H. Lange

Langley Aeronautical Laboratory
Langley Air Force Base, Va.

NATIONAL ADVISORY COMMITTEE
FOR AERONAUTICS

WASHINGTON
July 6, 1950

NATIONAL ADVISORY COMMITTEE FOR AERONAUTICS

RESEARCH MEMORANDUM

MAXIMUM-LIFT CHARACTERISTICS OF A WING WITH THE LEADING-EDGE SWEEPBACK DECREASING FROM 45° AT THE ROOT TO 20° AT THE TIP AT REYNOLDS NUMBERS FROM 2.4×10^6 TO 6.0×10^6

By Roy H. Lange

SUMMARY

Results are presented of an investigation of the maximum-lift characteristics of a wing with the leading-edge sweepback decreasing from 45° at the root to 20° at the tip and having an aspect ratio of 4.12 and NACA 64A009 airfoil sections. The investigation was made for conditions of leading edge smooth and leading edge rough for the basic wing and for the wing with split flaps, leading-edge flaps, outboard slats, and combinations of these high-lift devices at Reynolds numbers from 2.4×10^6 to 6.0×10^6. The maximum lift coefficient at a Reynolds number of 4.84×10^6 is 0.86 for the basic wing, 1.30 with split flaps installed, 1.24 with full-span leading-edge flaps installed, and 1.66 for the combination of full-span leading-edge flaps and split flaps. A large amount of static longitudinal stability near maximum lift is indicated for all configurations except those with full-span leading-edge flaps where the stability is marginal. The full-span leading-edge flaps provide a considerable increase in the lift-drag ratio at high angles of attack. The results obtained for the subject wing are comparable to those obtained for conventional sweptback wings of moderate sweepback.

INTRODUCTION

Some consideration has been given to a sweptback wing with the sweep decreasing from root to tip as a means of alleviating the poor low-speed characteristics of sweptback wings. The selection of this particular plan form is based on the premise that the smaller angle of

sweepback in the outboard wing panels would diminish the inherent early tip-stalling tendencies and thus improve the low-speed stability and control characteristics. Tests at low scale of this type of sweptback wing (reference 1) show, for low-speed conditions, a linear variation of pitching-moment coefficient with lift coefficient to stall with a stable break at the stall, and increments in lift due to plain-flap deflection which are considerably higher than those measured for conventional sweptback wings. In view of these favorable results at low scale, a general investigation has been conducted in the Langley full-scale tunnel on a full-scale wing with the leading-edge sweepback decreased from 45° at the root to 30° at the midsemispan and to 20° at the tip. The wing has an aspect ratio of 4.12, a taper ratio of 0.36, and NACA 64A009 airfoil sections parallel to the plane of symmetry. The investigation included tests to determine the maximum-lift and stalling characteristics, the chordwise and spanwise pressure distributions, and the lateral stability characteristics of the wing for several flapped configurations.

Results are presented herein at low Mach numbers and high Reynolds numbers of the maximum-lift characteristics of the basic wing and of the wing with split flaps, leading-edge flaps, outboard slats, and combinations of these high-lift devices. The effects of leading-edge roughness were investigated, and the scale effect on the aerodynamic characteristics was determined for a range of Reynolds number from about 2.4×10^6 to 6.0×10^6.

COEFFICIENTS AND SYMBOLS

The data are referred to the wind axes with the origin at the quarter chord of the mean aerodynamic chord. The data have been reduced to standard NACA nondimensional coefficients which are defined as follows:

C_L lift coefficient $\left(\frac{\text{Lift}}{qS}\right)$

C_D drag coefficient $\left(\frac{\text{Drag}}{qS}\right)$

C_m pitching-moment coefficient $\left(\frac{M}{qS\bar{c}}\right)$

R Reynolds number $\left(\frac{\rho V\bar{c}}{\mu}\right)$

$C_{L_{max}}$	maximum lift coefficient
$\frac{c_l c}{C_L' c_{av}}$	span loading coefficient
C_L'	lift coefficient as determined from pressure distributions
c_l	section lift coefficient
α	angle of attack, degrees
$\alpha_{C_{L_{max}}}$	angle of attack for maximum lift, degrees
q	free-stream dynamic pressure
S	wing area (190.24 sq ft)
ρ	mass density of air
M	pitching moment
V	free-stream velocity
μ	coefficient of viscosity
$\bar{c}$	mean aerodynamic chord measured parallel to plane of symmetry (7.28 ft) $\left(\frac{2}{S}\int_0^{b/2} c^2 dy\right)$
c	chord, parallel to plane of symmetry
c_{av}	average chord $\left(\frac{S}{b}\right)$
b	wing span
y	spanwise coordinate
δ_f	split-flap deflection, degrees
λ	taper ratio

Λ angle of sweepback at leading edge, degrees

A aspect ratio

MODEL

The geometric characteristics of the wing and the arrangement of the high-lift devices are given in figures 1 and 2. Photographs of the wing mounted in the Langley full-scale tunnel are given as figure 3. The airfoil section of the wing is the NACA 64A009 parallel to the plane of symmetry. The wing-tip shape is one-half of a body of revolution of the airfoil section. The wing has no geometric dihedral or twist.

The wing construction consisted of a simple framework of $\frac{1}{4}$-inch steel channel spars and ribs covered with a $\frac{1}{8}$-inch skin of aluminum sheet rolled to the correct airfoil contour. The juncture in the region of the wing leading edge where two panels of different sweepback intersected was filled and rounded slightly and the entire wing surface was smooth and fair. The wing construction was rigid and it is believed that deflections of the wing were negligible during the tests. The split flaps were made of sheet metal attached to the wing under surface for flap deflections of 30°, 45°, and 60° measured from the wing chord line as shown in figure 2(b). The leading-edge flaps were made of sheet metal welded to a 1.5-inch-diameter steel tube, and flap spans of 35, 70, and 100 percent of the wing span measured from the wing tip were provided. (See fig. 2(a).) The design of the slat (fig. 2(c)) was determined from the results of two-dimensional tests reported in reference 2. Inasmuch as the slat is not retractable into the wing leading edge, it therefore does not represent a true slat installation; however, it is felt that the data are representative of the effects of the slat on the aerodynamic characteristics of the wing.

For the tests with the leading edge rough, No. 60 (0.011-inch mesh) carborundum grains were applied to a thin layer of shellac over a surface length of 8 percent chord measured from the leading edge parallel to the plane of symmetry on both upper and lower wing surfaces. The grains covered 5 to 10 percent of the affected area. For the tests with the leading-edge flaps installed, the roughness was applied only to the upper surface of the flap and around the flap leading edge.

TESTS

All tests were made through an angle-of-attack range from about -2° through stall in increments of 2° except near maximum lift, where 1° increments were used. Force measurements were made to determine the lift, the drag, and the pitching moment for conditions of leading edge smooth and leading edge rough of the basic wing and of the wing with split flaps, leading-edge flaps, outboard slats, and for combinations of these high-lift devices. The scale effect on the aerodynamic characteristics of the wing was determined from tests made at various tunnel airspeeds to give a Reynolds number range of from about 2.4×10^6 to 6.0×10^6. The highest Mach number obtained in the tests was 0.13 at a Reynolds number of 6.0×10^6.

The stalling characteristics were determined from visual observation and from motion-picture records of the action of wool tufts attached to the upper wing surface. These tuft studies were made at Reynolds numbers of about 3.5×10^6 and 4.8×10^6, both for conditions of leading edge smooth and leading edge rough.

Preliminary tests were made to determine the effect of a change in gap between the slat and the wing leading edge from the position shown in figure 2(c) to a position in which the slat was moved forward 5/8 inch parallel to the wing chord line. Although this change in slat gap produced no appreciable change in the longitudinal characteristics of the wing, the flow in the region of the slat was unsteady, and for this reason all slat tests were made with the slat as shown in figure 2(c).

PRESENTATION OF DATA

The data have been corrected for the stream alinement, the blocking effects, and the jet-boundary effects which were calculated on the basis of an unswept wing. No tests were made to determine the support tare and interference effects on the longitudinal characteristics; however, all investigations of wings made recently on the same wing supports have shown these effects to be negligible.

The figures covering the maximum-lift results are outlined to facilitate the discussion. The test data are presented in the figures given in the following table:

Configuration	Reynolds number range	δ_f (deg)	Leading-edge condition	Figure
Basic wing	2,460,000 to 6,020,000	0	Smooth and rough	4
Split flaps installed	3,500,000	30, 45, 60	Smooth	5
Split flaps installed	2,390,000 to 5,800,000	60	Smooth and rough	6
Leading-edge flaps installed, 35-percent span	2,400,000 to 4,980,000	0	Smooth	7
Leading-edge flaps installed, 70-percent span	2,440,000 to 4,890,000	0	Smooth	8
Leading-edge flaps installed, full span	2,360,000 to 4,900,000	0	Smooth and rough	9
Leading-edge flaps installed, 35-percent span	2,440,000 to 4,950,000	60	Smooth	10
Leading-edge flaps installed, 70-percent span	2,310,000 to 4,620,000	60	Smooth	11
Leading-edge flaps installed, full span	2,340,000 to 4,780,000	60	Smooth and rough	12
Leading-edge slat installed	2,490,000 to 4,880,000	0	Smooth	13
Leading-edge slat installed	2,320,000 to 4,700,000	60	Smooth	14

Stall diagrams for the more important configurations are given in figures 15 and 16. Data obtained from pressure-distribution measurements over the basic wing (reference 3) are given in figure 17 to aid in the analysis. Summary curves of the effects of varying the leading-edge-flap span on the longitudinal characteristics of the wing given in figures 18 and 19 were derived from the data of figures 7 to 12. A summary of the variation of $C_{L_{max}}$ with Reynolds number for the more important configurations with both smooth and rough leading edge is given in figure 20.

RESULTS AND DISCUSSION

Basic-Wing Characteristics

The maximum lift coefficient (as defined by the portion of the lift curve where the lift initially levels off) of the basic wing is 0.86 at a Reynolds number of 4.84×10^6. (See fig. 4.) The lift curve is linear up to an angle of attack of about 12°, and a value of lift-curve slope of 0.0625 per degree is measured at a Reynolds number of 4.84×10^6. Although the wing has an unusual plan form, an attempt was made to predict the lift-curve slope utilizing the charts of reference 4. Using the sweep of the midsemispan panel of 30°, the data of reference 4 predict a lift-curve slope of 0.062 per degree, which is in good agreement with the experimental value at the higher Reynolds numbers.

For the straight-line portion of the lift curve the pitching-moment characteristics indicate that the wing is longitudinally stable, statically, for the center-of-gravity location selected (figs. 4(a) and 4(b)); however, as the lift curve rounds off at an angle of attack of 12.8° (at a Reynolds number of 3.51×10^6), the stall diagrams show the occurrence of leading-edge separation at the tips (fig. 15(a)), and the pitching-moment curves show a slight destabilizing tendency. (See figs. 4(a) and 4(b).) This destabilizing tendency results from a slight loss in loading of the tip sections and an inboard shift of the spanwise center of pressure as shown in the typical loading curves of figure 17. A small increase in angle of attack to 13.8° results in an unsteady, circular motion of the boundary-layer air on the upper wing surface proceeding from the inboard end of the midsemispan panel toward the outboard end, and then in a direction opposite to that of the free stream toward the leading edge. (See

fig. 15(a).) Except for rough flow, the flow over the tip sections has not greatly changed from that for the previous angle of attack, and the lift of the tip sections is maintained; however, as shown in figure 17, there is a loss in loading at the midsemispan panel and a rearward shift in the local center of pressure. As shown by the stall diagrams and loading curves, these effects continue with increasing angle of attack and, together with the rearward shift in local center of pressure at the midsemispan panel caused by leading-edge separation (at $\alpha = 14.7^\circ$), produce increasingly negative pitching moments through the angle of attack for maximum lift ($\alpha = 15.7^\circ$). Accordingly, the pitching-moment curves show a large amount of static longitudinal stability at maximum lift for the center of gravity selected. (See fig. 4(b).)

Effects of Split-Flap Deflection

The increment in lift coefficient due to split-flap deflection at zero angle of attack is 0.58 at $\delta_f = 60^\circ$, and the corresponding increment in maximum lift coefficient is 0.43. (See fig. 5(a).) As the maximum lift coefficient of the wing is the same for the split-flap deflections of 45° and 60°, the deflection of 45° is considered optimum because of the smaller drag. However, this result was not apparent from the preliminary studies of the wing; therefore, all subsequent data were obtained with a split-flap deflection of 60°.

Except for the usual change in trim, split-flap deflection caused no appreciable change in the variation of pitching-moment coefficient with lift coefficient as compared with the basic wing; however, the destabilizing tendency prior to maximum lift is more pronounced for a flap deflection of 60°. (See fig. 5(c).) As is shown subsequently, however, this effect is modified with increasing Reynolds number. The indicated satisfactory low-speed static longitudinal stability of the wing with split flaps deflected is also significant, for the results of references 5 and 6 show that the instability at the stall for wings of 42° and 34° sweepback and of about the same aspect ratio is intensified by the addition of split flaps.

The stall diagrams for the wing with split flaps deflected 60° show about the same stall progression as was noted for the basic-wing configuration. (See figs. 16(a) and 15(a).)

Effects of Leading-Edge Flaps

Lift characteristics.- The effects of varying the leading-edge-flap span on the maximum-lift characteristics presented in figure 18(a) were obtained from the data of figures 7 to 12. These results show

that the major portion of the total increase in maximum lift obtained with full-span leading-edge flaps installed is contributed by the extension of the flaps over the midsemispan panel. The maximum lift coefficient of the wing with full-span leading-edge flaps installed is increased to 1.24 with split flaps removed and to 1.66 with split flaps installed at a Reynolds number of about 4.80×10^6. (See fig. 18(a).) These values of maximum lift coefficient are from 0.36 to 0.38 higher than those obtained for the corresponding wing configurations without leading-edge flaps installed. These increases are due not only to a delay of the stalling to higher angles of attack as compared with the wing without leading-edge flaps installed, but also to an increase in wing area, which has not been taken into account in the calculation of the wing coefficients.

The stall diagrams of the wing with the full-span leading-edge flaps installed alone (fig. 15(b)) show that rough flow initially occurs at the wing trailing edge in the outer semispan at a comparatively high angle of attack, as compared with the initial rough flow at the leading edge for the basic wing. A spanwise flow of the boundary-layer air begins at the wing trailing edge at an angle of attack of 18.4°, and for a further increase in angle of attack of only 1° the unsteady type of flow described previously for the basic wing is shown over a large portion of the wing. The circular-flow pattern occurs in the outboard spanwise sections at the angle of attack for maximum lift and then shifts slightly inboard after the stall. The addition of split flaps to the full-span leading-edge-flap configuration results in an abrupt stall. (See fig. 16(b).) At an angle of attack of 17.8° only a small amount of roughness is indicated at the junctures between panels of different sweepback, and maximum lift is obtained at this point. For an increase in angle of attack of only 1° the flow becomes rough and unsteady over about 75 percent of the span and there is a sharp drop in lift. A stall progression of this type is considered undesirable for it would give no stall warning, and a slight asymmetry near stall may lead to serious rolling instability.

It should be noted that these full-span leading-edge-flap configurations were sensitive to local discontinuities at the flap leading edge and at the juncture of the flap and wing which resulted in asymmetric stalling; therefore, the force measurements were made only after tuft studies had revealed a symmetrical stall.

Pitching-moment characteristics.- The effect of varying the leading-edge-flap span on the variations of pitching-moment coefficient with lift coefficient given in figure 18(b) shows no significant change in the static longitudinal stability as compared with the basic wing until the flap span increases beyond 0.70b/2. At lift coefficients below the stall, the progression of flow separation from the trailing edge forward (fig. 15(b)), combined with the added wing area at the

leading edge, causes a forward shift in the wing aerodynamic center such that only a slight amount of longitudinal stability is indicated for the wing with full-span leading-edge flaps installed alone. (See fig. 18(b).) The occurrence of the previously mentioned unsteady flow at maximum lift results in marginal stability through the stall. With split flaps installed the pitching-moment curves indicate a fair degree of static longitudinal stability for the combinations of both the 0.70b/2 leading-edge flaps and split flaps and the full-span leading-edge flaps and split flaps (fig. 18(b)). The stability is marginal at the stall for both configurations.

Drag characteristics.- As shown by the variations of C_L with C_D given in figure 19, the full-span leading-edge flaps provide a considerable increase in the lift-drag ratio of the wing at the high angles of attack both with split flaps installed and removed.

Effects of Leading-Edge Slats

The function of the slats is to maintain unstalled flow over the tip sections up to angles of attack greater than the stall angle for the basic wing, and, as shown by the stall diagrams of figures 15(c) and 16(c), this effect is obtained with the slats. The improved flow over the tip sections with 0.35b/2 slats installed, however, (figs. 13(a) and 14(a)) results in only small increases in maximum lift coefficient because of flow breakdown induced at the inboard end of the slats. The increases in maximum lift coefficient of less than 0.10 are of the same magnitude as those obtained with the 35-percent-span leading-edge flaps installed. (See fig. 18(a).) In general, the pitching-moment characteristics are similar to those obtained for the basic wing and the wing with split flaps installed. (See figs. 13(b) and 14(b).)

Effects of Reynolds Number and Roughness

Maximum lift.- The maximum lift coefficient is increased only slightly for all wing configurations with increase in Reynolds number from about 2.4×10^6 to 5.9×10^6. (See fig. 20.) Leading-edge roughness causes no appreciable change in maximum lift coefficient at the lowest Reynolds numbers but decreases the maximum lift coefficient by about 0.10 at the highest Reynolds numbers investigated for all configurations. (See fig. 20.) Tuft observations showed that leading-edge roughness had no appreciable effect on the stall progression of the wing for all configurations investigated except that the initial change from undisturbed flow occurred at somewhat lower angles of attack than for the smooth leading-edge condition.

Pitching moment.- In general, the effect of increasing Reynolds number on the pitching-moment characteristics is to delay the slight destabilizing tendency obtained at moderate lift coefficients to higher lift coefficients and to provide a more uniform variation of C_m with C_L. (See figs. 4(b), 6(b), 9(b), and 12(b).) For the combination of the full-span leading-edge flap and split flaps (fig. 12(b)) the adverse break in the pitching-moment curve at stall at a Reynolds number of 3.47×10^6 is alleviated at a Reynolds number of 4.69×10^6. The effect of leading-edge roughness is to alleviate the destabilizing tendency obtained at moderate lift coefficients for the basic wing and wing with split flaps deflected 60°, especially at the high Reynolds numbers. With full-span leading-edge flaps and split flaps installed, roughness caused nose-up pitching moments even at the highest Reynolds number. (See fig. 12(b).)

Drag.- The effect of leading-edge roughness on the drag coefficient of the basic wing (fig. 4(c)) and wing with split flaps installed (fig. 6(c)) is to decrease the angle of attack above which a rapid drag rise occurs by about 5° at the highest Reynolds numbers investigated; however, this effect is not shown at the lowest Reynolds number. With full-span leading-edge flaps installed, leading-edge roughness produced no increase in drag at the higher angles of attack up to stall, both with split flaps removed and installed. (See figs. 9(c) and 12(c).) The improvement in lift-drag ratio provided by the leading-edge flap shown in figure 19, therefore, will not be appreciably changed by leading-edge roughness.

Comparison of Results with Those for Conventional Sweptback Wings

An evaluation of the low-speed characteristics of the subject wing must be based primarily on the experience gained from tests of numerous sweptback-wing configurations since no truly comparable data are available. The maximum lift coefficient of the basic wing of 0.86 at $R = 4.84 \times 10^6$ is of about the correct magnitude when compared with the data for wings of aspect ratio 4.5 and NACA 64A010 airfoil sections which show maximum lift coefficients of 0.92 and 0.88, respectively, for an increase in sweepback from 11.8° to 38.0° (references 7 and 8).

A study of the low-speed longitudinal stability boundary of sweptback wings given in reference 9 shows that for an aspect ratio of 4.12, the maximum angle of sweepback to obtain longitudinal stability is about 35°. The satisfactory static longitudinal stability of the subject wing, therefore, is in accord with what would be expected from consideration of wing geometry, since the small part of the wing having sweep

greater than 35° would not be expected to have much effect. With the present sweep arrangement the aspect ratio could probably be increased to 5 and possibly 6.

The split flaps provide a considerable increase in the lift of the wing throughout the angle-of-attack range, and the values of ΔC_L at zero angle of attack and $\Delta C_{L_{max}}$ are given in the following table along with the data ($\delta_f = 60°$) from several sweptback wings for a range of sweepback and aspect ratio.

Wing	Λ (deg)	λ	A	Airfoil section	Flap span, b/2	ΔC_L at $\alpha = 0°$	$\Delta C_{L_{max}}$
Reference 6	34	0.44	4.84	[1]NACA 0015 root NACA 23009 tip	0.623	0.58	0.45
Reference 10	37.25	.50	6.00	[1]NACA 64_1-212	.65	.51	.33
Unpublished	47.5	.50	3.4	[1]NACA 64_1A112	.65	.39	.08
Unpublished	47.72	.38	5.1	[1]NACA 64-210	.62	.40	.06
Reference 6	49	.42	3.64	[1]NACA 0015 root NACA 23009 tip	.623	.43	.11
Subject wing	45 to 20	.36	4.12	NACA 64A009	.65	.58	.43

[1]Airfoil sections not parallel to plane of symmetry.

The results show that the data for the subject wing are more representative of those obtained for wings of moderate sweepback. As compared with an unswept wing of the same aspect ratio and taper ratio, calculations based on the methods of reference 11 show that the increment in lift coefficient at a point 3° below stall is only 10 percent greater for the unswept wing.

SUMMARY OF RESULTS

The results of an investigation at high Reynolds numbers and low Mach numbers in the Langley full-scale tunnel of the maximum-lift characteristics of a wing with the leading-edge sweepback decreasing from 45° at the root to 20° at the tip are summarized as follows:

1. The maximum lift coefficient of the basic wing is 0.86 at a Reynolds number of 4.84×10^6, and the tuft observations show that the lifting capabilities of the basic wing are limited because of the occurrence of leading-edge separation. The addition of 65-percent-span split flaps deflected 60° increases the maximum lift coefficient to 1.30.

The maximum lift coefficient of the wing with full-span leading-edge flaps installed is 1.24, and the addition of the split flaps to this configuration increases this value to 1.66.

2. A large amount of static longitudinal stability is indicated for the wing near maximum lift for all configurations except those with the full-span leading-edge flaps installed or with the combination of the 0.70b/2 leading-edge flaps and split flaps where the static longitudinal stability is marginal.

3. The full-span leading-edge flaps provide a considerable increase in the lift-drag ratio at the high angles of attack, both with split flaps installed and removed.

4. Leading-edge roughness decreases the maximum lift coefficient by about 0.10 at the highest Reynolds numbers investigated for all configurations but has no significant effect on the pitching-moment characteristics except for the combination of full-span leading-edge flaps and 65-percent-span split flaps where nose-up moments were obtained at the stall.

5. Increasing Reynolds number causes only a slight increase in maximum lift coefficient of the smooth wing and has no appreciable effect on the pitching-moment characteristics.

6. The outboard 35-percent-span slat and leading-edge flap both provide about the same slight improvement in the longitudinal aerodynamic characteristics of the wing.

7. The results obtained for the subject wing are comparable to those obtained for conventional sweptback wings of moderate sweepback.

Langley Aeronautical Laboratory
National Advisory Committee for Aeronautics
Langley Air Force Base, Va.

REFERENCES

1. Krüger, W.: Six-Component Measurements on a Cranked Swept-Back Wing. Reps. and Translations No. 816, British M.A.P. Völkenrode, Jan. 15, 1947.

2. Gottlieb, Stanley M.: Two-Dimensional Wind-Tunnel Investigation of Two NACA 6-Series Airfoils with Leading-Edge Slats. NACA RM L8K22, 1949.

3. Barnett, U. Reed, Jr., and Lange, Roy H.: Low-Speed Pressure-Distribution Measurements at a Reynolds Number of 3.5×10^6 on a Wing with Leading-Edge Sweepback Decreasing from 45° at the Root to 20° at the Tip. NACA RM L50A23a, 1950.

4. DeYoung, John: Theoretical Additional Span Loading Characteristics of Wings with Arbitrary Sweep, Aspect Ratio, and Taper Ratio. NACA TN 1491, 1947.

5. Neely, Robert H., and Conner, D. William: Aerodynamic Characteristics of a 42° Swept-Back Wing with Aspect Ratio 4 and NACA 641-112 Airfoil Sections at Reynolds Numbers from 1,700,000 to 9,500,000. NACA RM L7D14, 1947.

6. McCormack, Gerald M., and Stevens, Victor I., Jr.: An Investigation of the Low-Speed Stability and Control Characteristics of Swept-Forward and Swept-Back Wings in the Ames 40- by 80-Foot Wind Tunnel. NACA RM A6K15, 1947.

7. Tinling, Bruce E., and Dickson, Jerald K.: Tests of a Model Horizontal Tail of Aspect Ratio 4.5 in the Ames 12-Foot Pressure Wind Tunnel. I - Quarter-Chord Line Swept Back 35°. NACA RM A9G13, 1949.

8. Tinling, Bruce E., and Dickson, Jerald K.: Tests of a Model Horizontal Tail of Aspect Ratio 4.5 in the Ames 12-Foot Pressure Wind Tunnel. II - Elevator Hinge Line Normal to the Plane of Symmetry. NACA RM A9H11a, 1949.

9. Shortal, Joseph A., and Maggin, Bernard: Effect of Sweepback and Aspect Ratio on Longitudinal Stability Characteristics of Wings at Low Speeds. NACA TN 1093, 1946.

10. Koven, William, and Graham, Robert R.: Wind-Tunnel Investigation of High-Lift and Stall-Control Devices on a 37° Sweptback Wing of Aspect Ratio 6 at High Reynolds Numbers. NACA RM L8D29, 1948.

11. Silverstein, Abe, and Katzoff, S.: Design Charts for Predicting Downwash Angles and Wake Characteristics behind Plain and Flapped Wings. NACA Rep. 648, 1939.

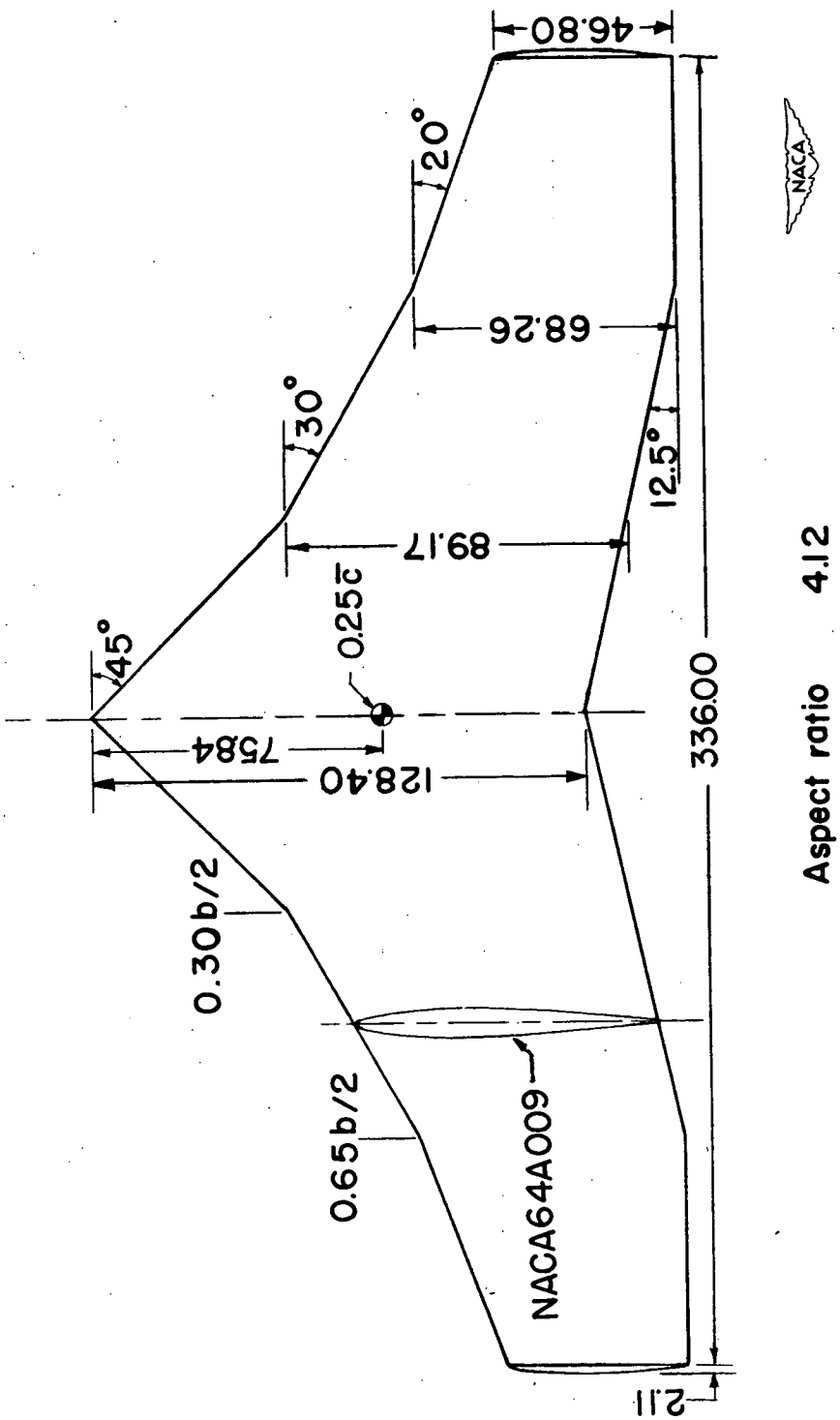

Figure 1.- Geometric characteristics of wing. All dimensions are given in inches.

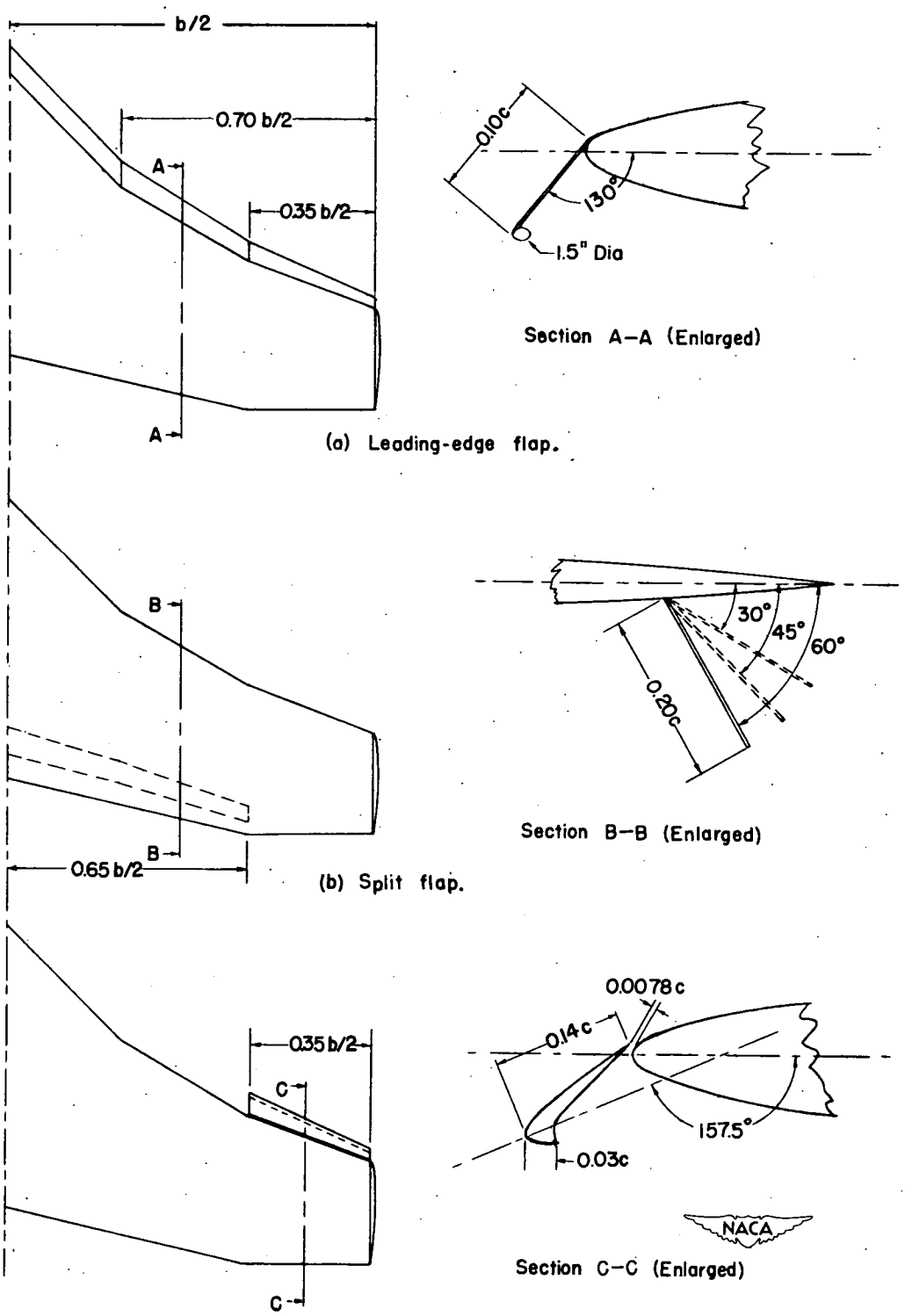

Figure 2.- Arrangement of high-lift devices investigated.

Page intentionally left blank

Page intentionally left blank

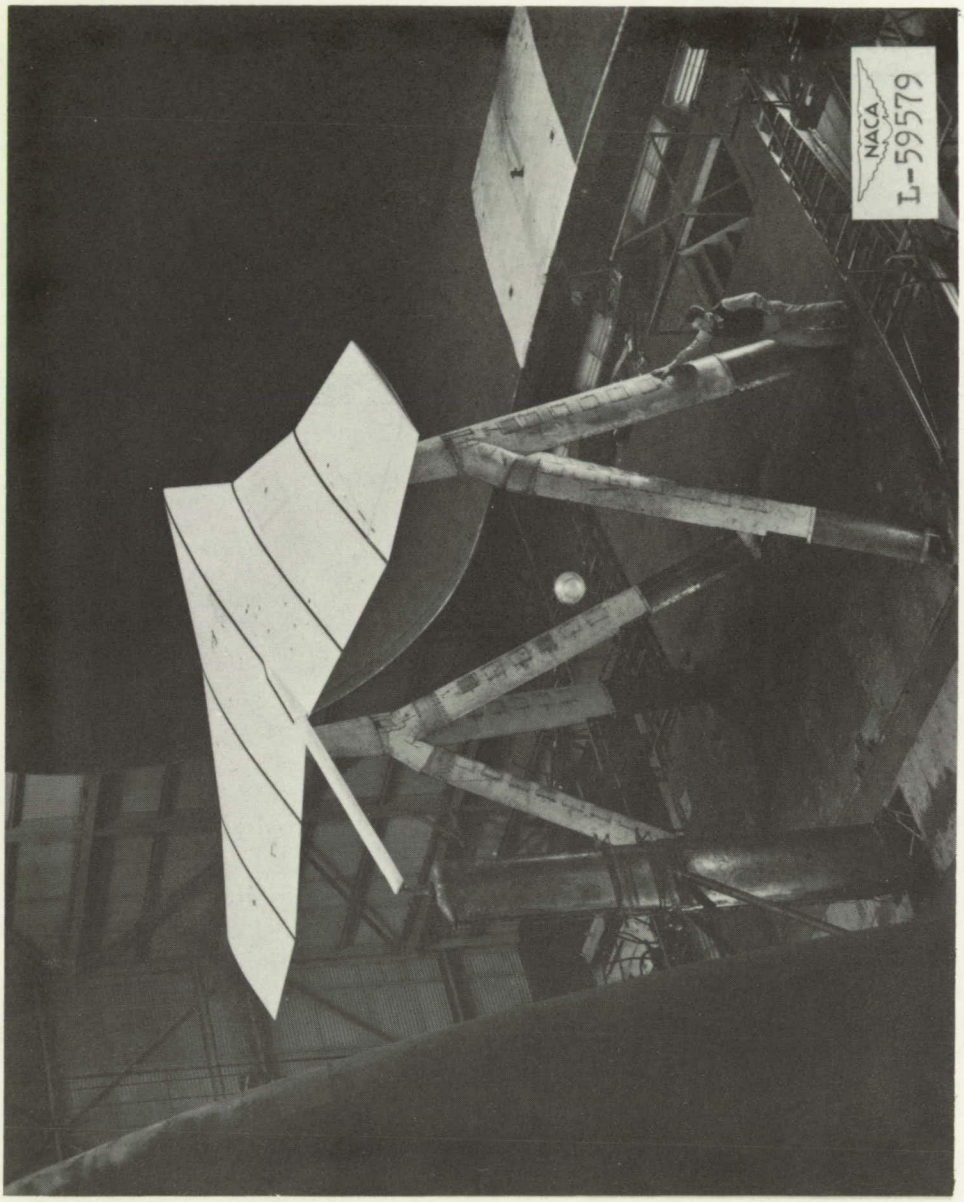

(a) Basic wing.

Figure 3.- Photographs of wing mounted in the Langley full-scale tunnel.

Page intentionally left blank

Page intentionally left blank

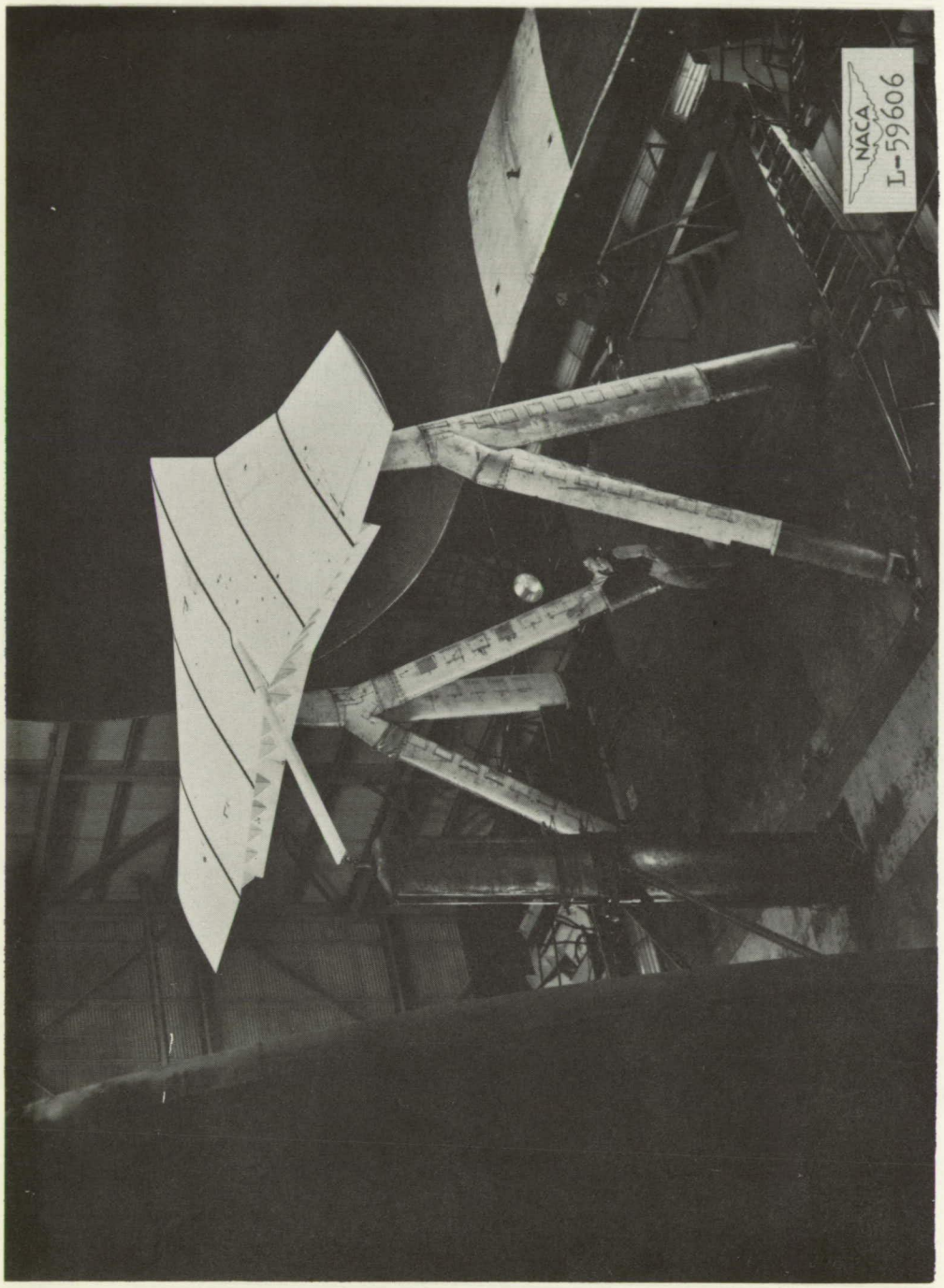

(b) Split flaps installed. $\delta_f = 60°$.

Figure 3.- Concluded.

Page intentionally left blank

Page intentionally left blank

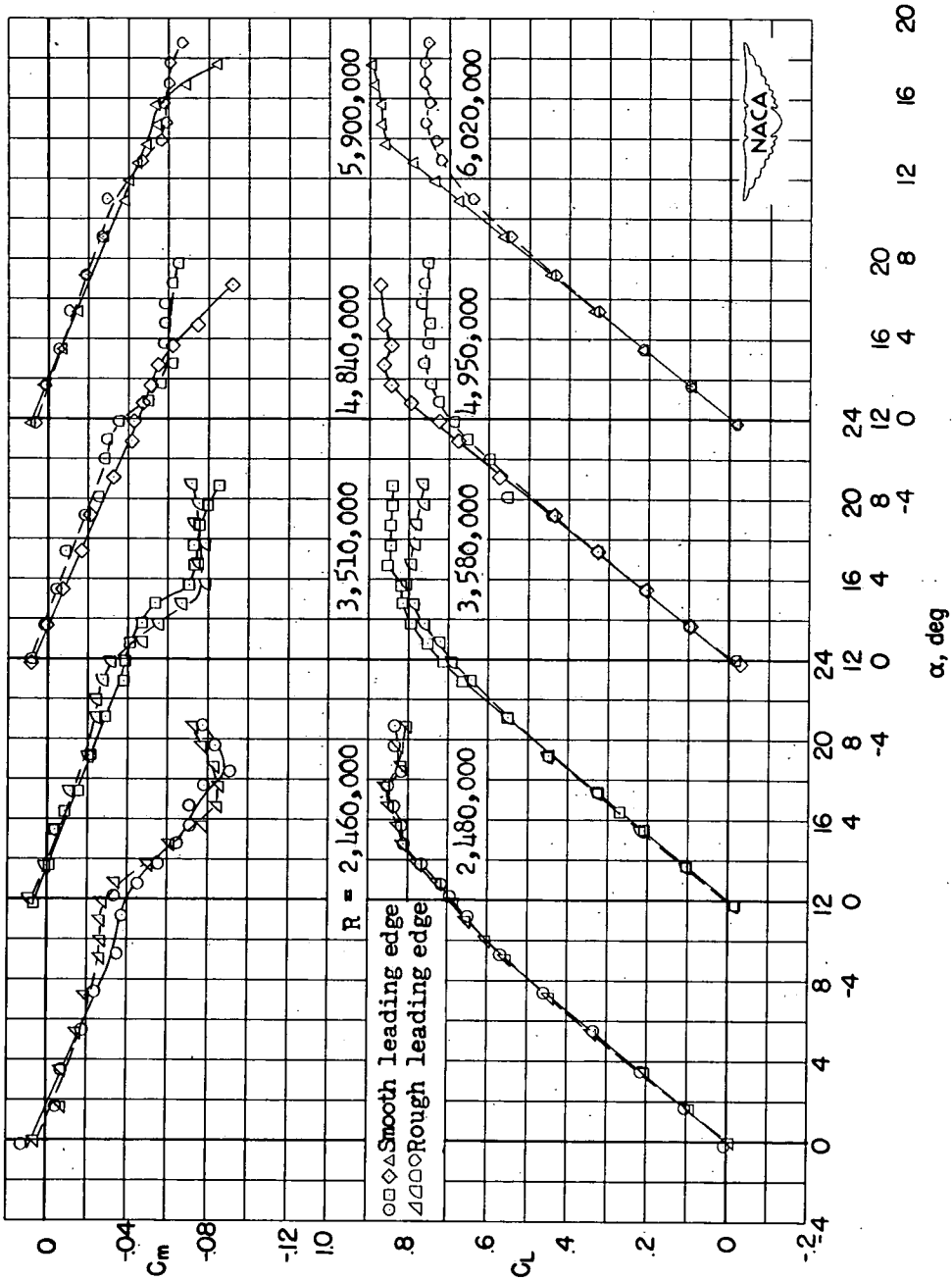

(a) Variation of C_L and C_m with α.

Figure 4.- Effects of Reynolds number and leading-edge roughness on the aerodynamic characteristics of the basic wing.

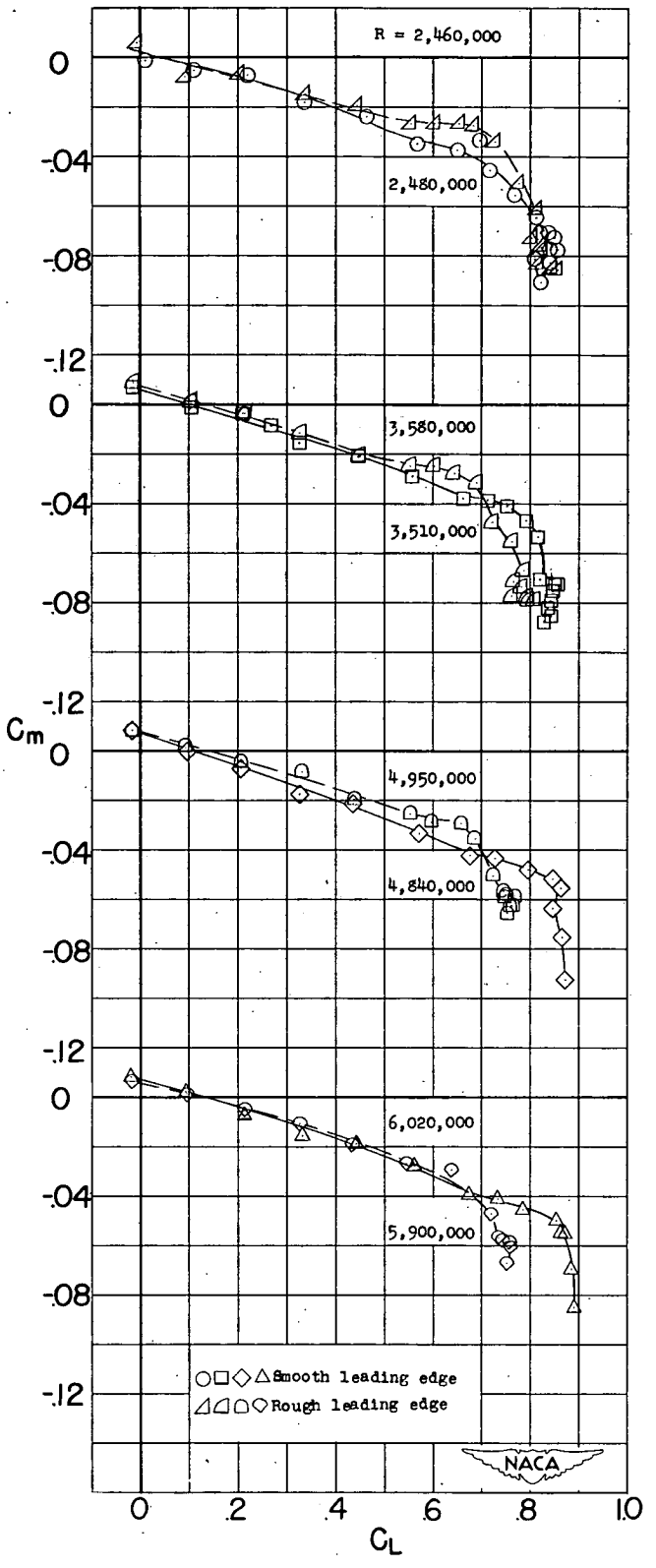

(b) Variation of C_m with C_L.

Figure 4.- Continued.

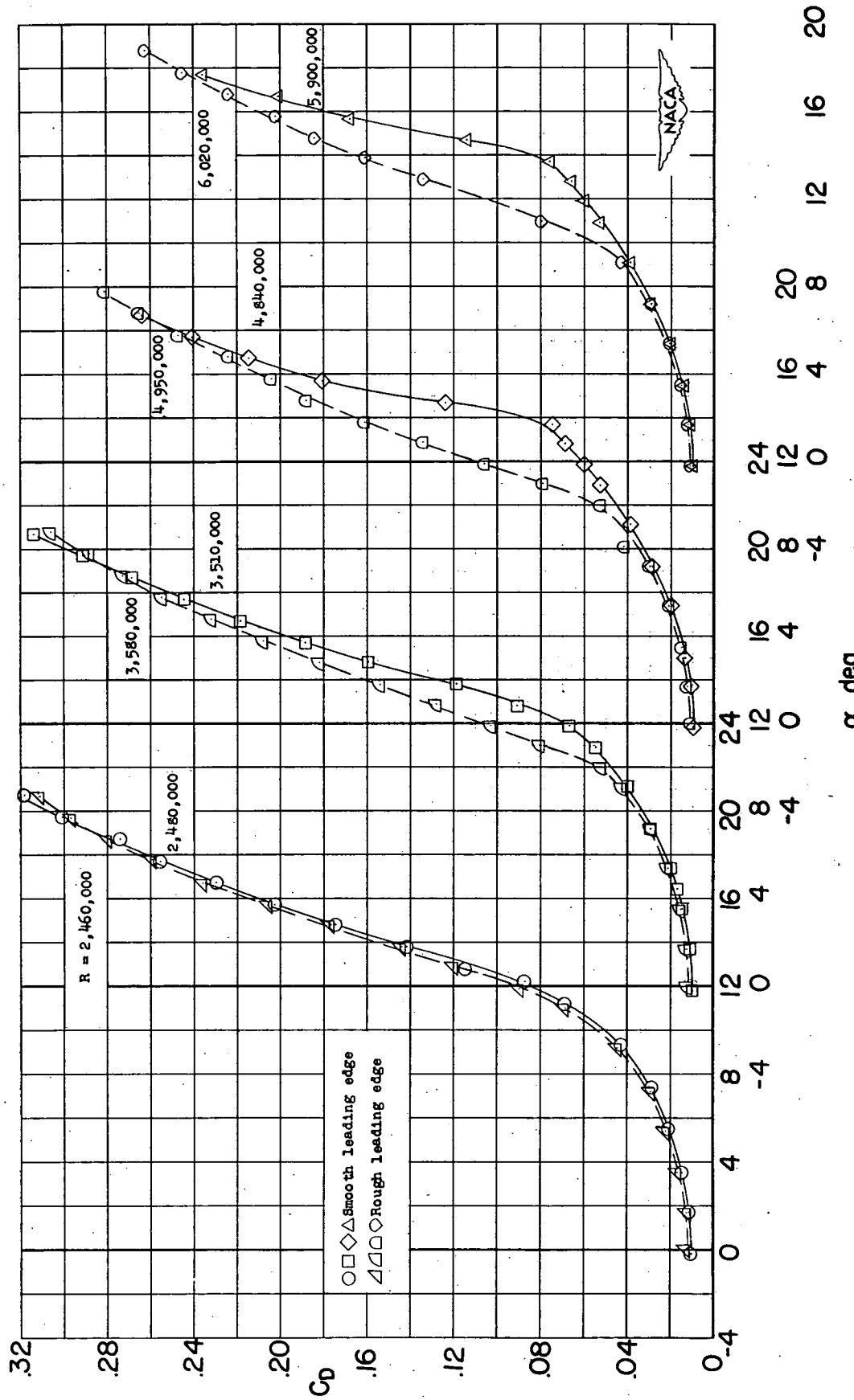

(c) Variation of C_D with α.

Figure 4.- Concluded.

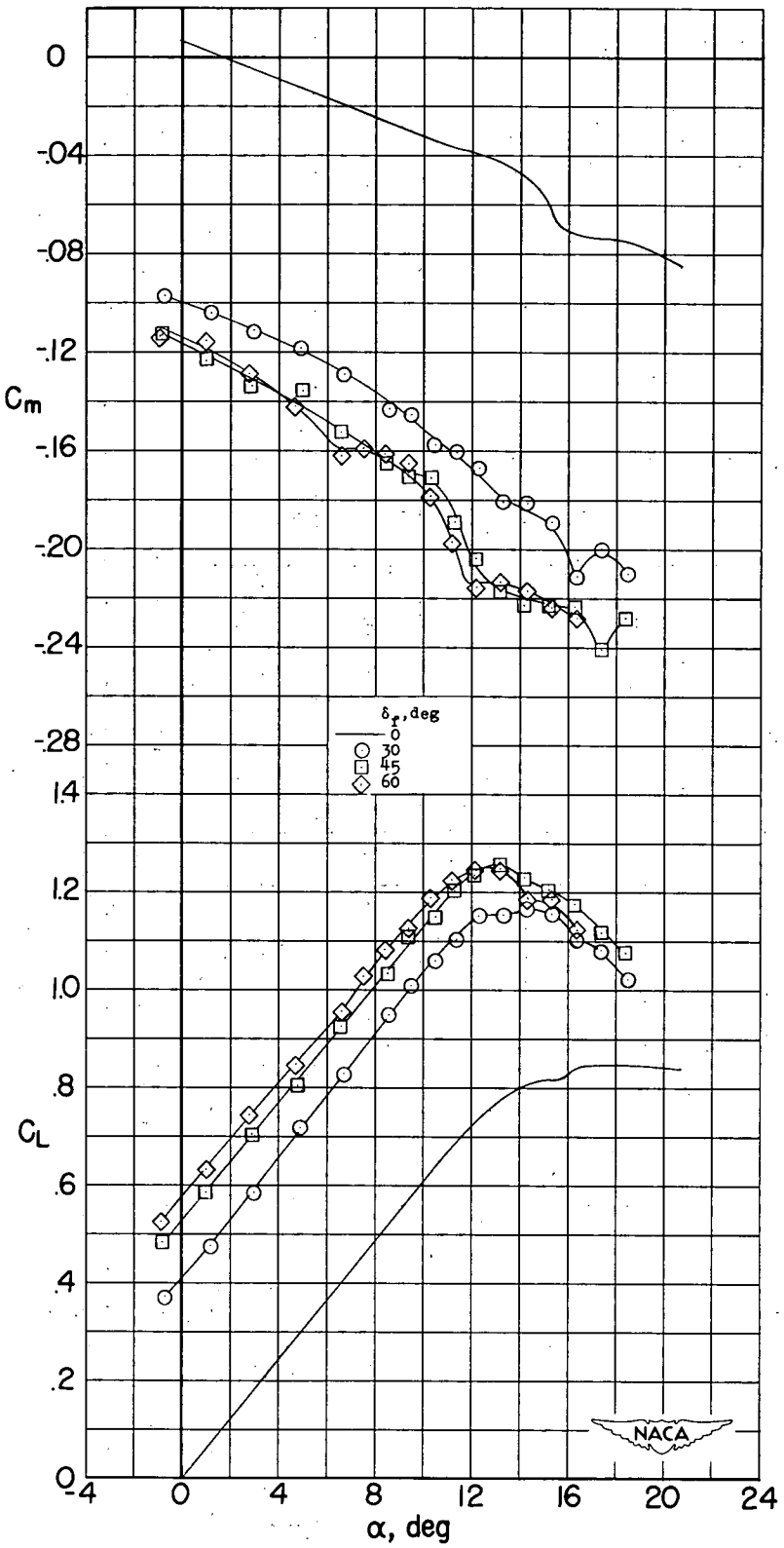

(a) Variation of C_L and C_m with α.

Figure 5.- Effect of split-flap deflection on the aerodynamic characteristics. $R \approx 3.5 \times 10^6$.

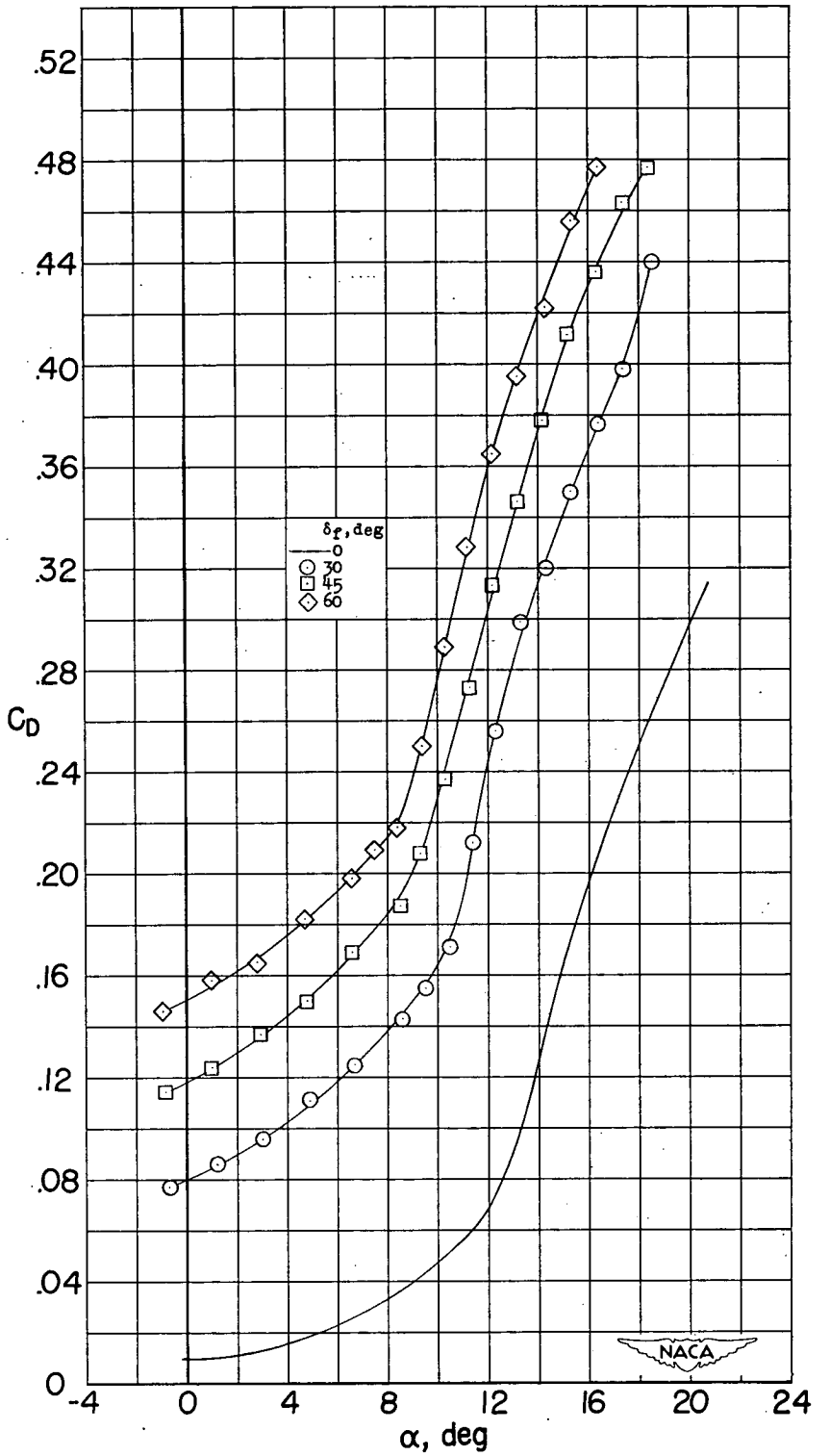

(b) Variation of C_D with α.

Figure 5.- Continued.

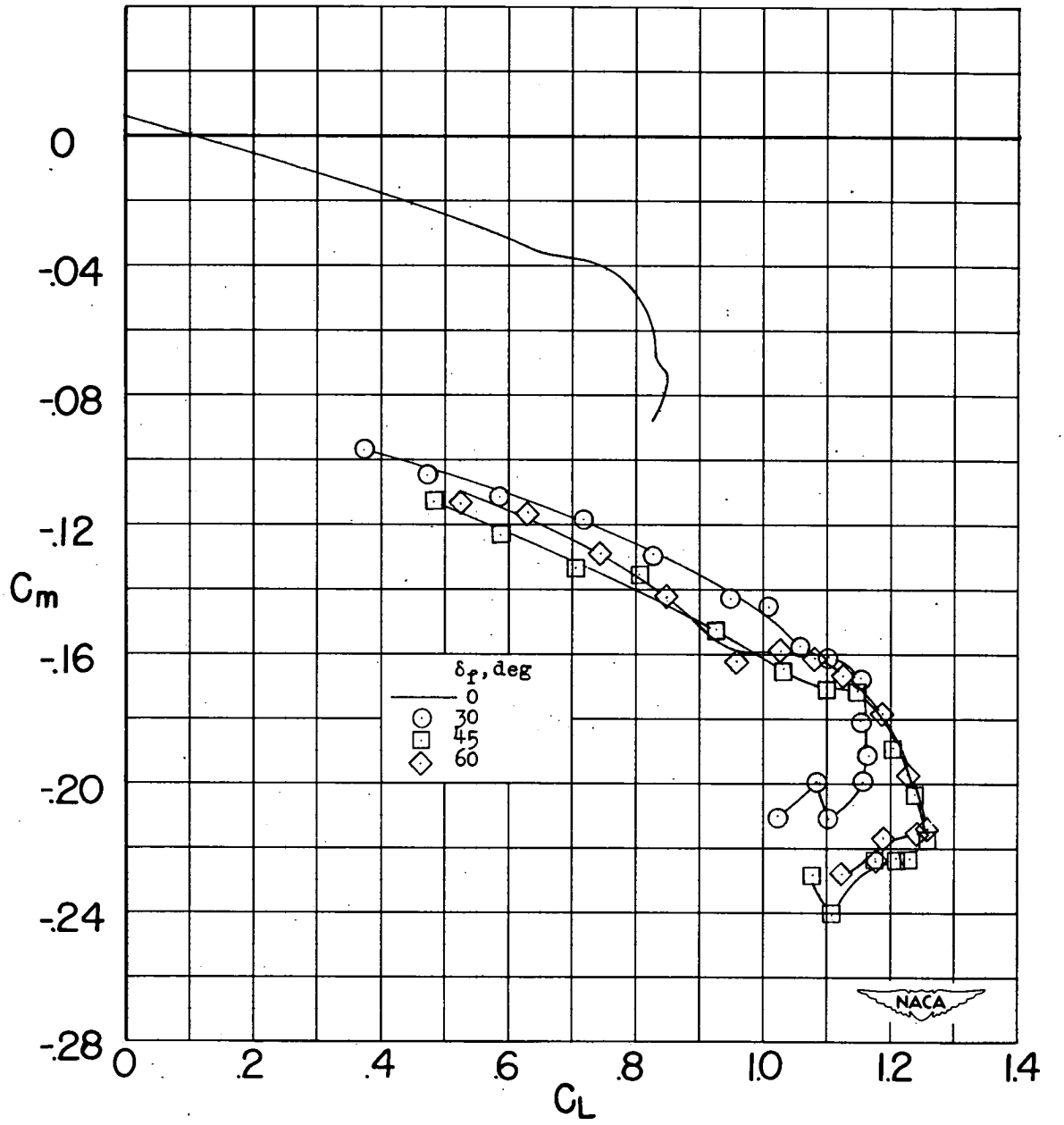

(c) Variation of C_m with C_L.

Figure 5.- Concluded.

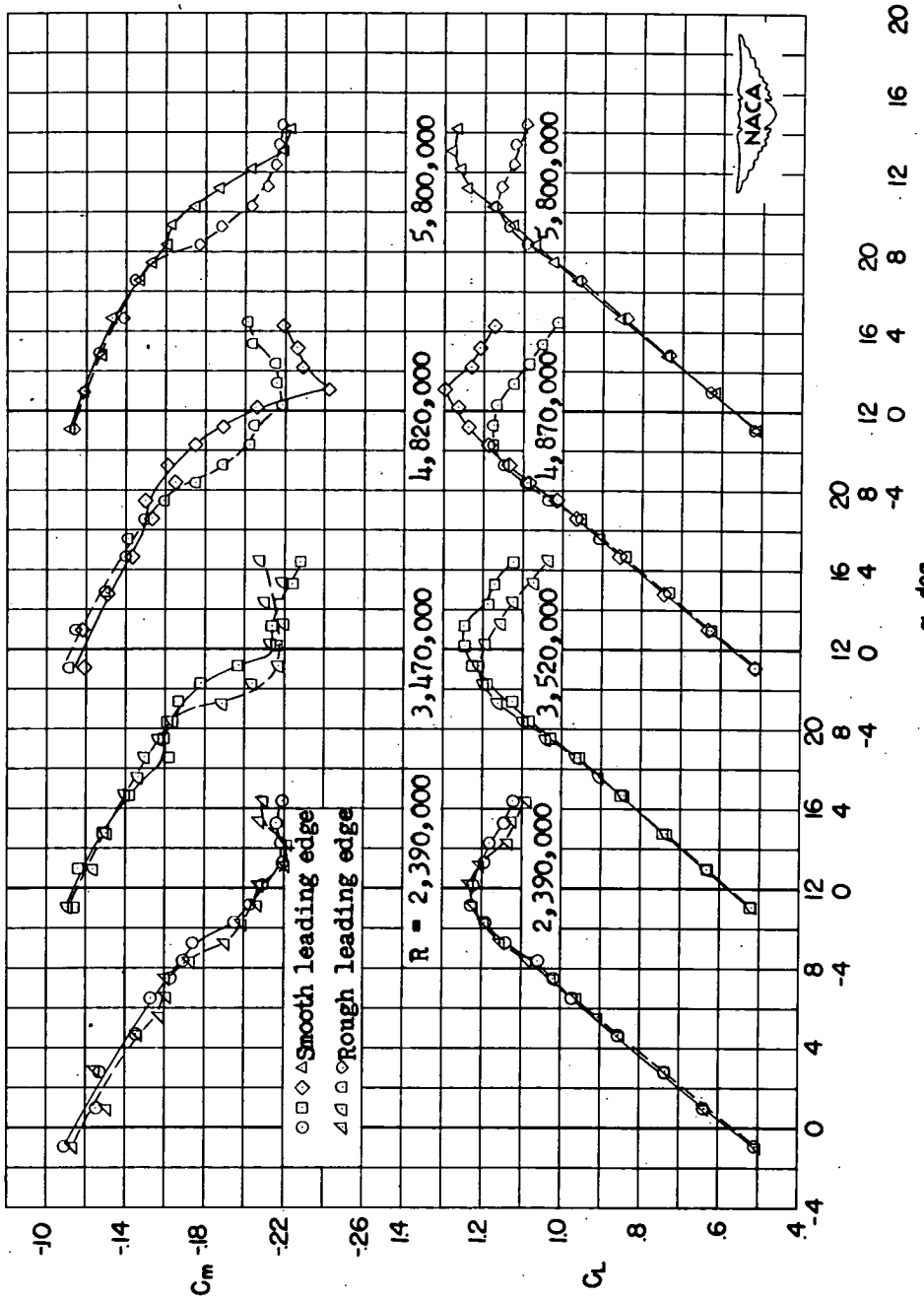

(a) Variation of C_L and Cm with α.

Figure 6.- Effects of Reynolds number and leading-edge roughness on the aerodynamic characteristics of the wing with 65-percent-span split flaps deflected 60°.

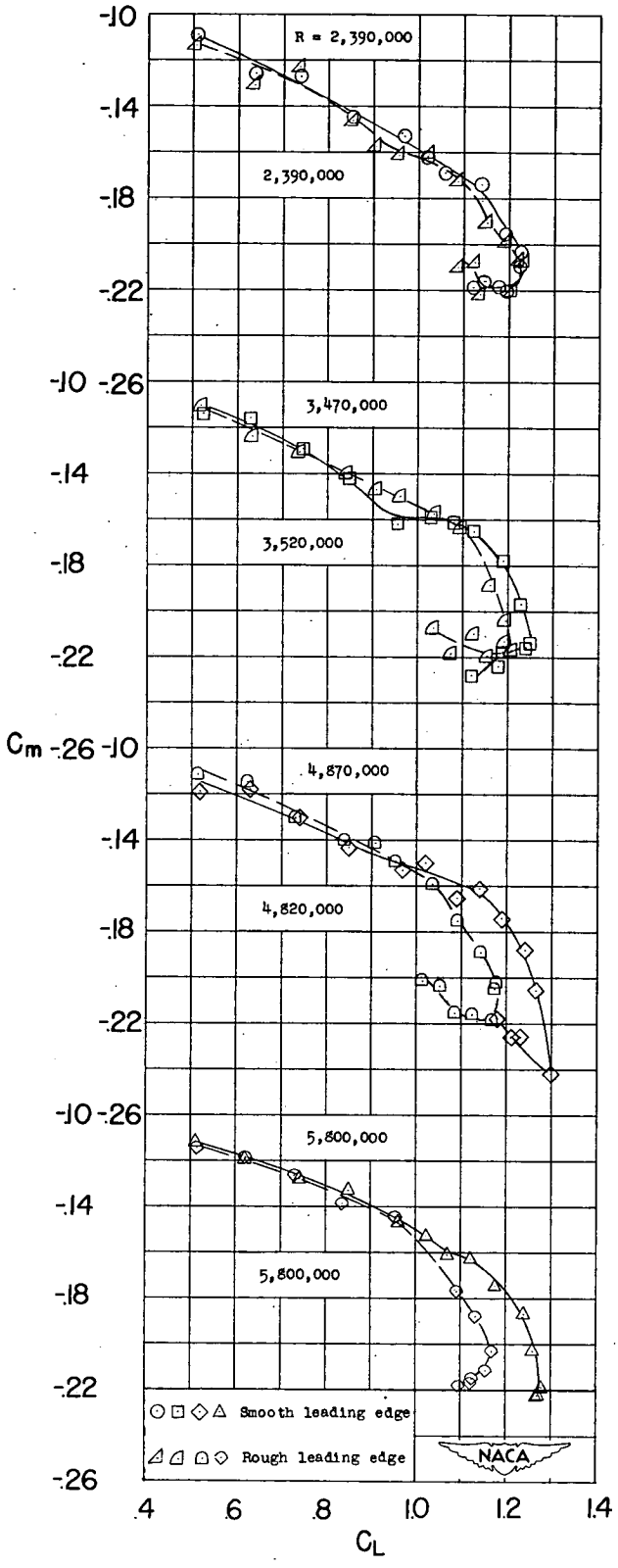

(b) Variation of C_m with C_L.

Figure 6.- Continued.

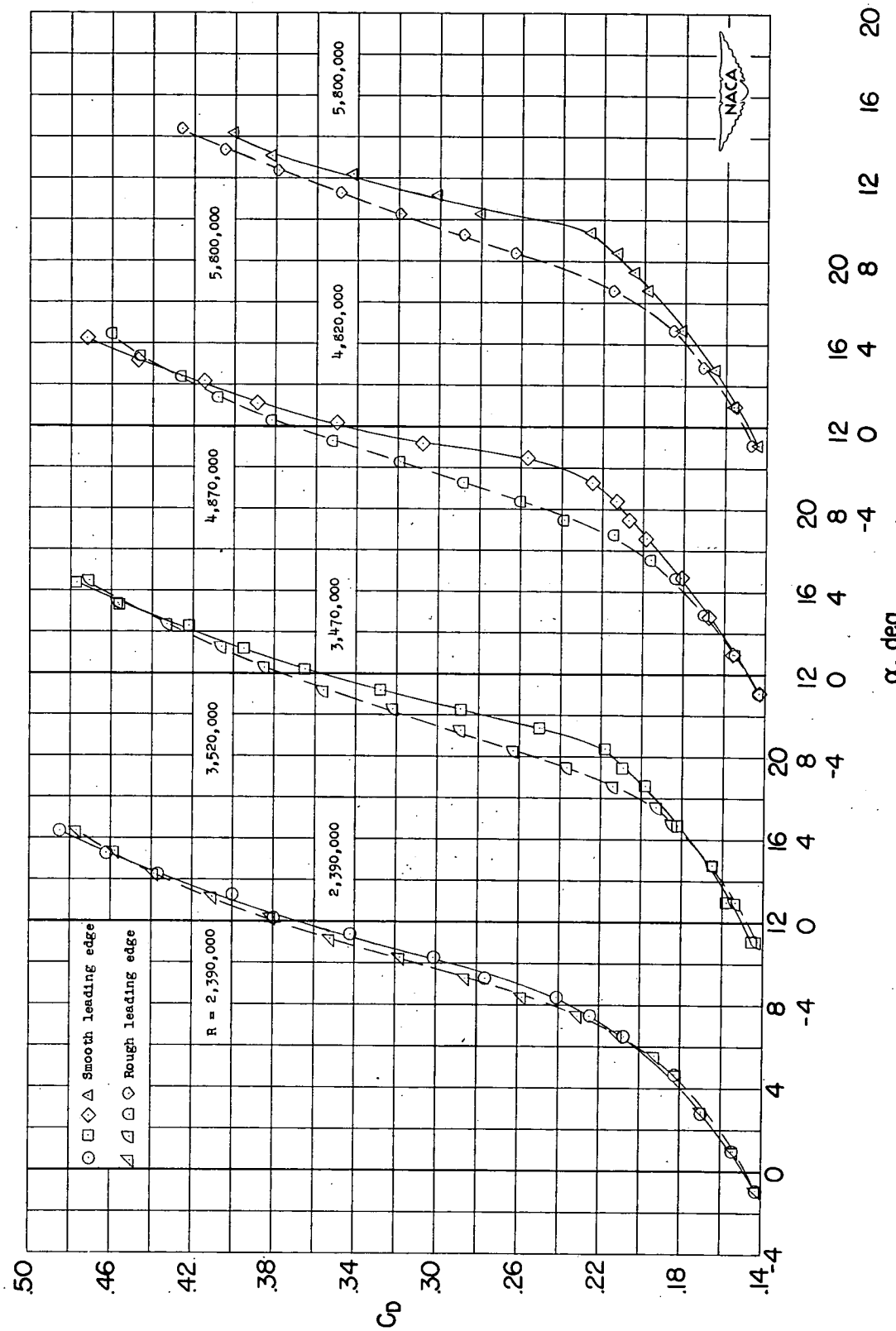

(c) Variation of C_D with α.

Figure 6.- Concluded.

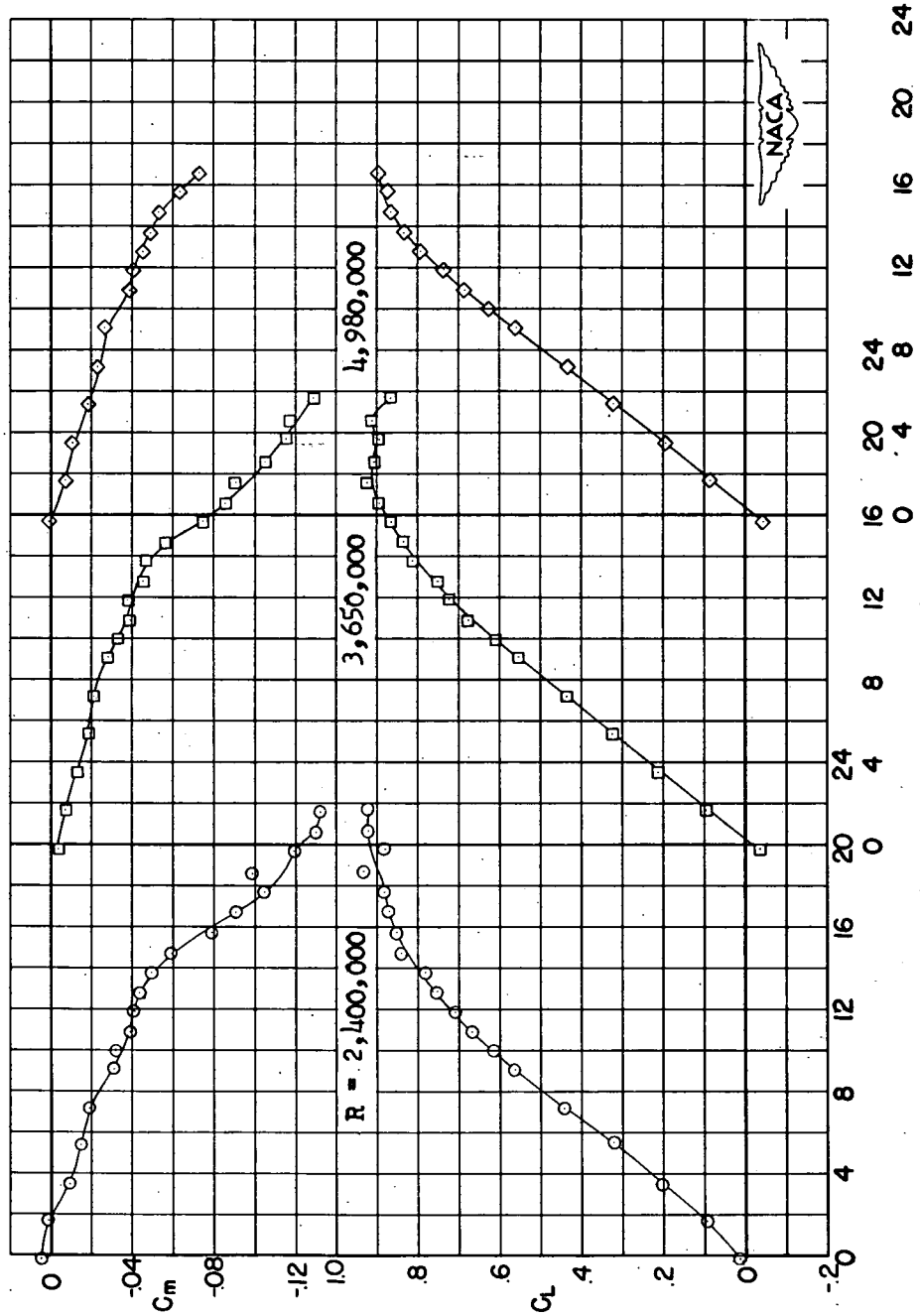

(a) Variation of C_L and C_m with α.

Figure 7.- Effect of Reynolds number on the aerodynamic characteristics of the wing with 35-percent-span leading-edge flaps. $\delta_f = 0^\circ$.

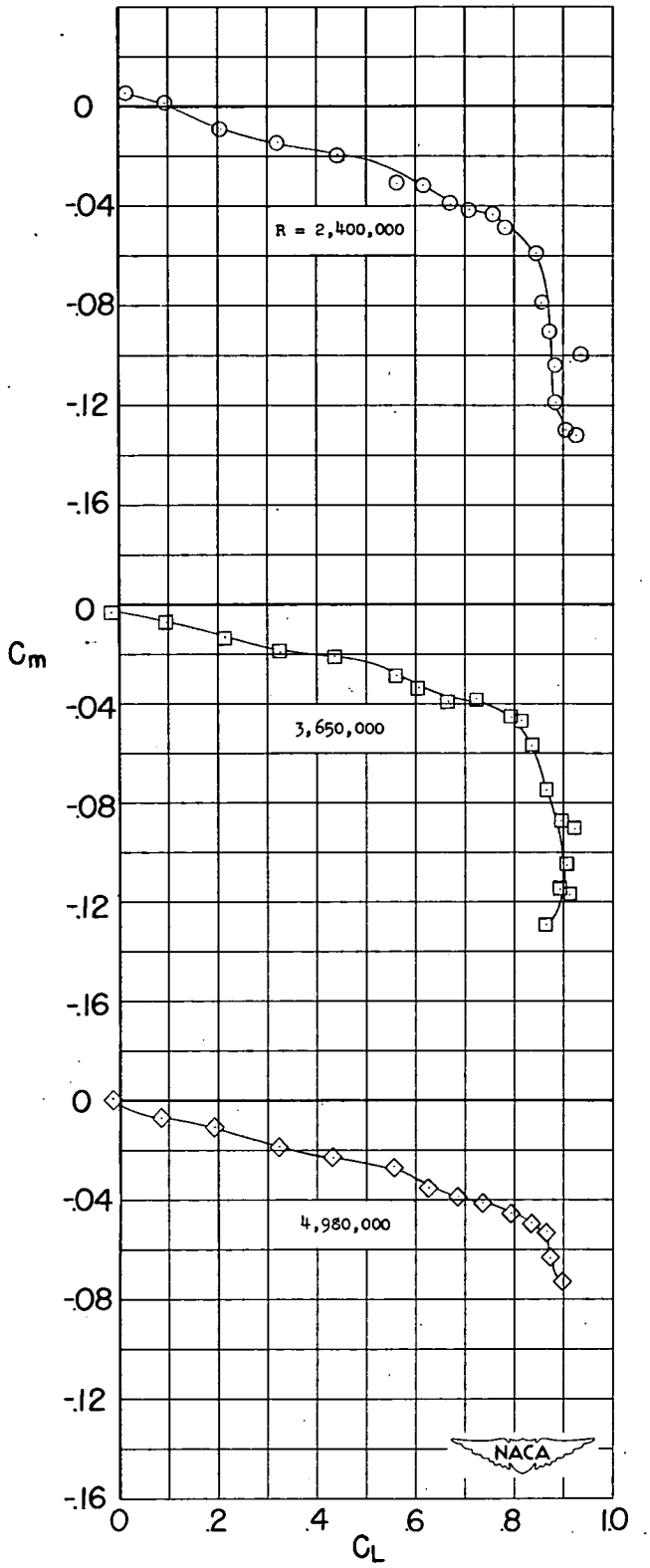

(b) Variation of C_m with C_L.

Figure 7.- Continued.

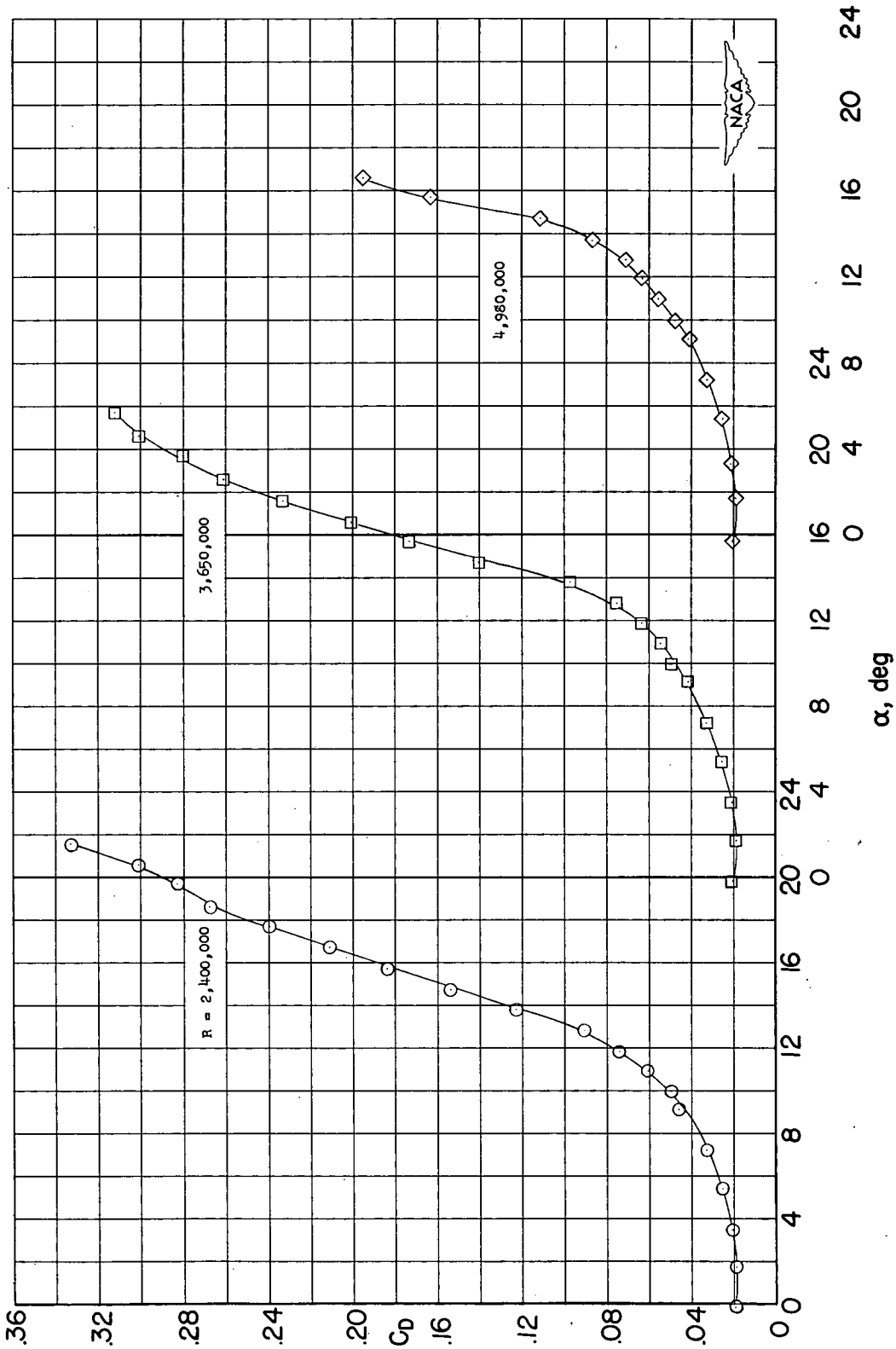

(c) Variation of C_D with α.

Figure 7.- Concluded.

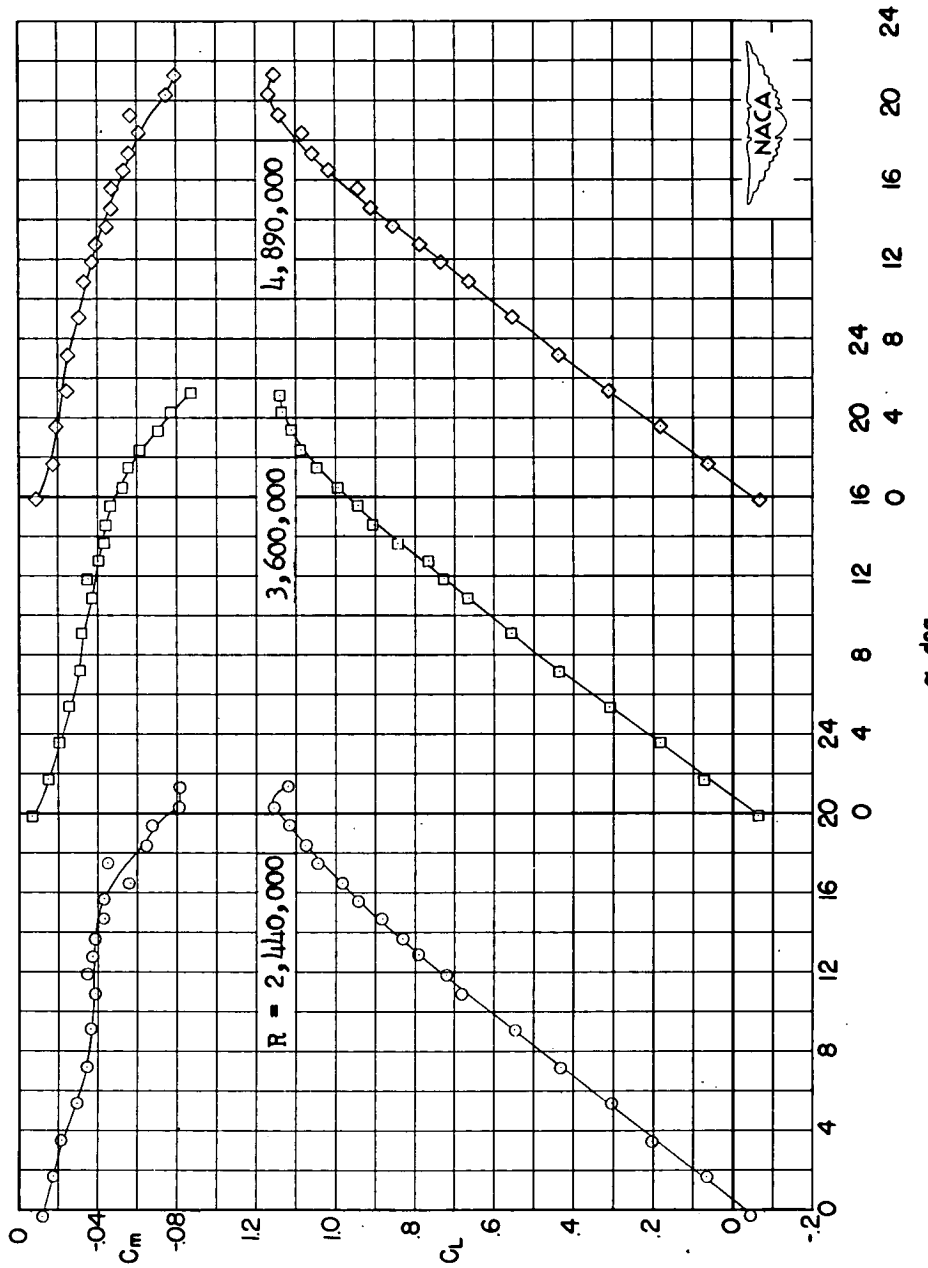

(a) Variation of C_L and C_m with α.

Figure 8.- Effect of Reynolds number on the aerodynamic characteristics of the wing with 70-percent-span leading-edge flaps. $\delta_f = 0^\circ$.

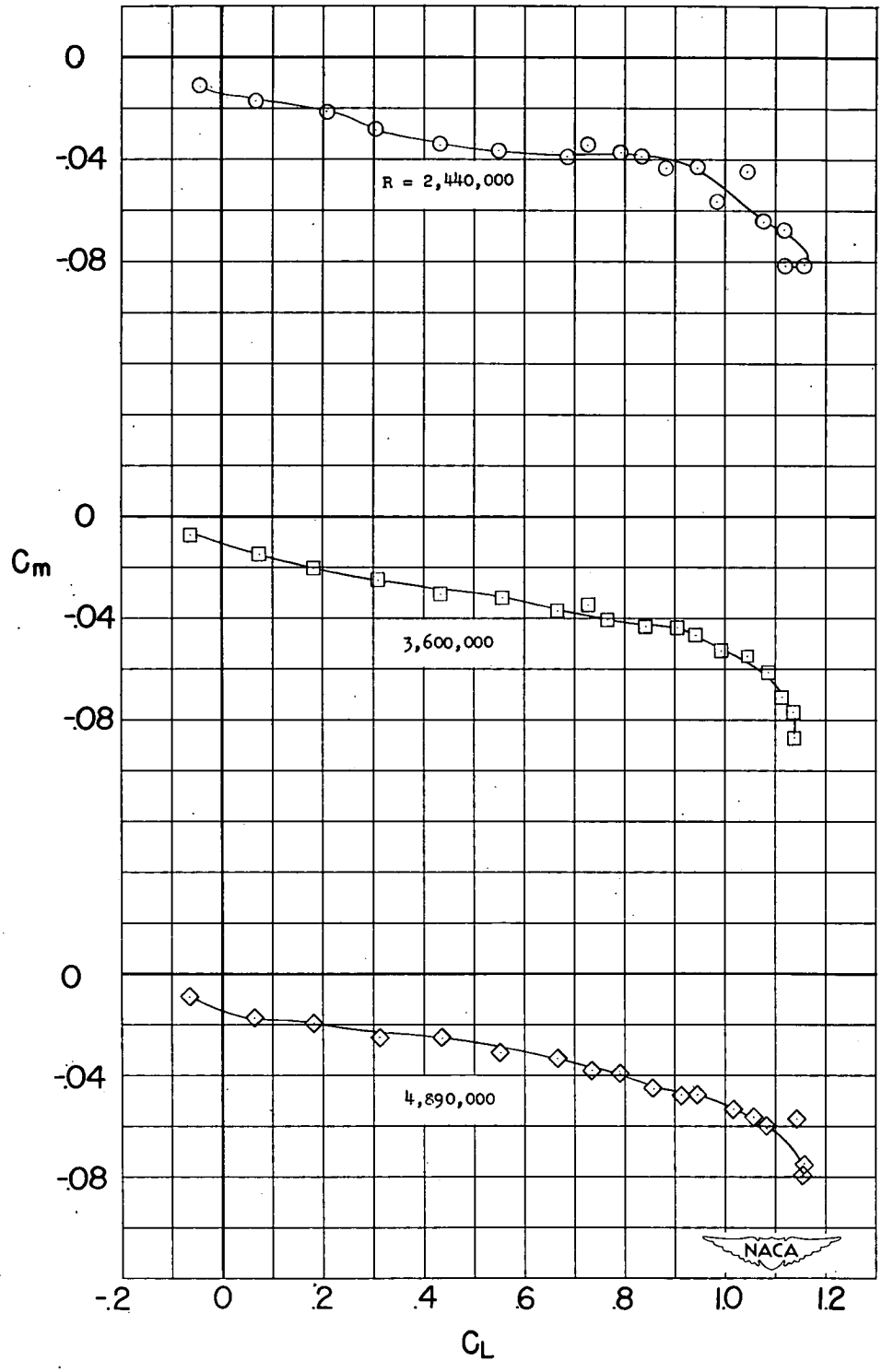

(b) Variation of C_m with C_L.

Figure 8.- Continued.

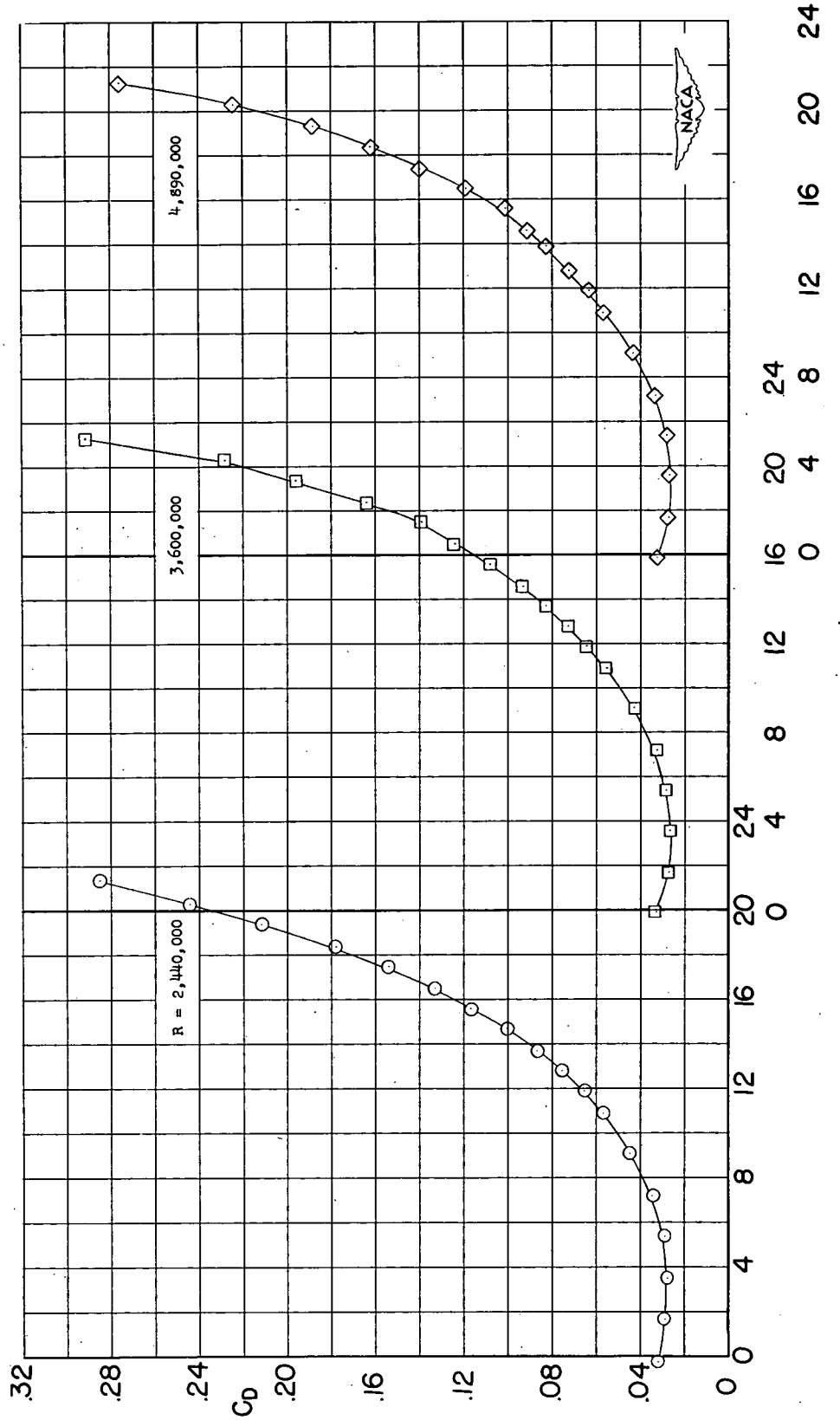

(c) Variation of C_D with α.

Figure 8.- Concluded.

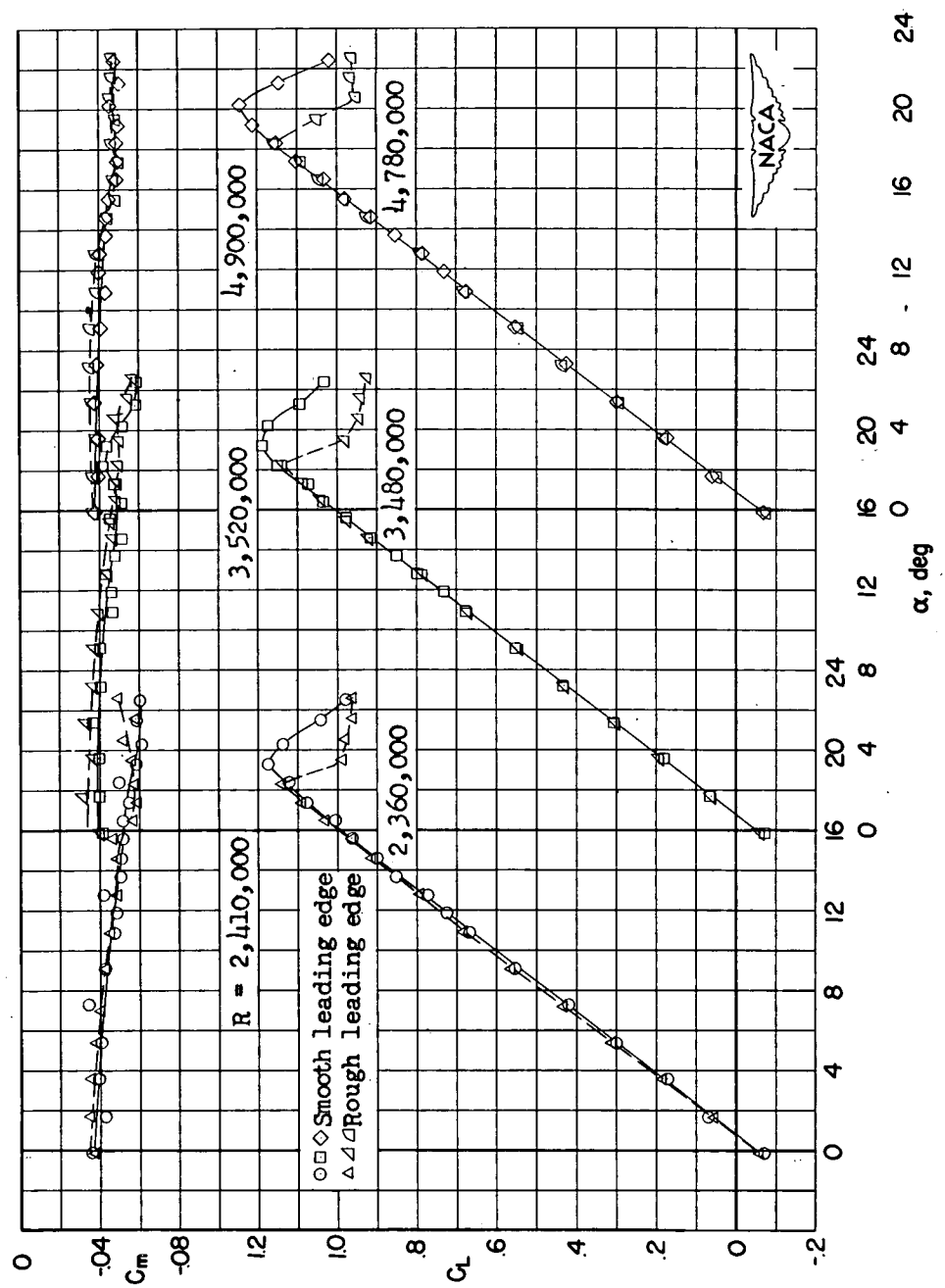

(a) Variation of C_L and C_m with α.

Figure 9.- Effect of Reynolds number and leading-edge roughness on the aerodynamic characteristics of the wing with full-span leading-edge flaps installed. $\delta_f = 0^\circ$.

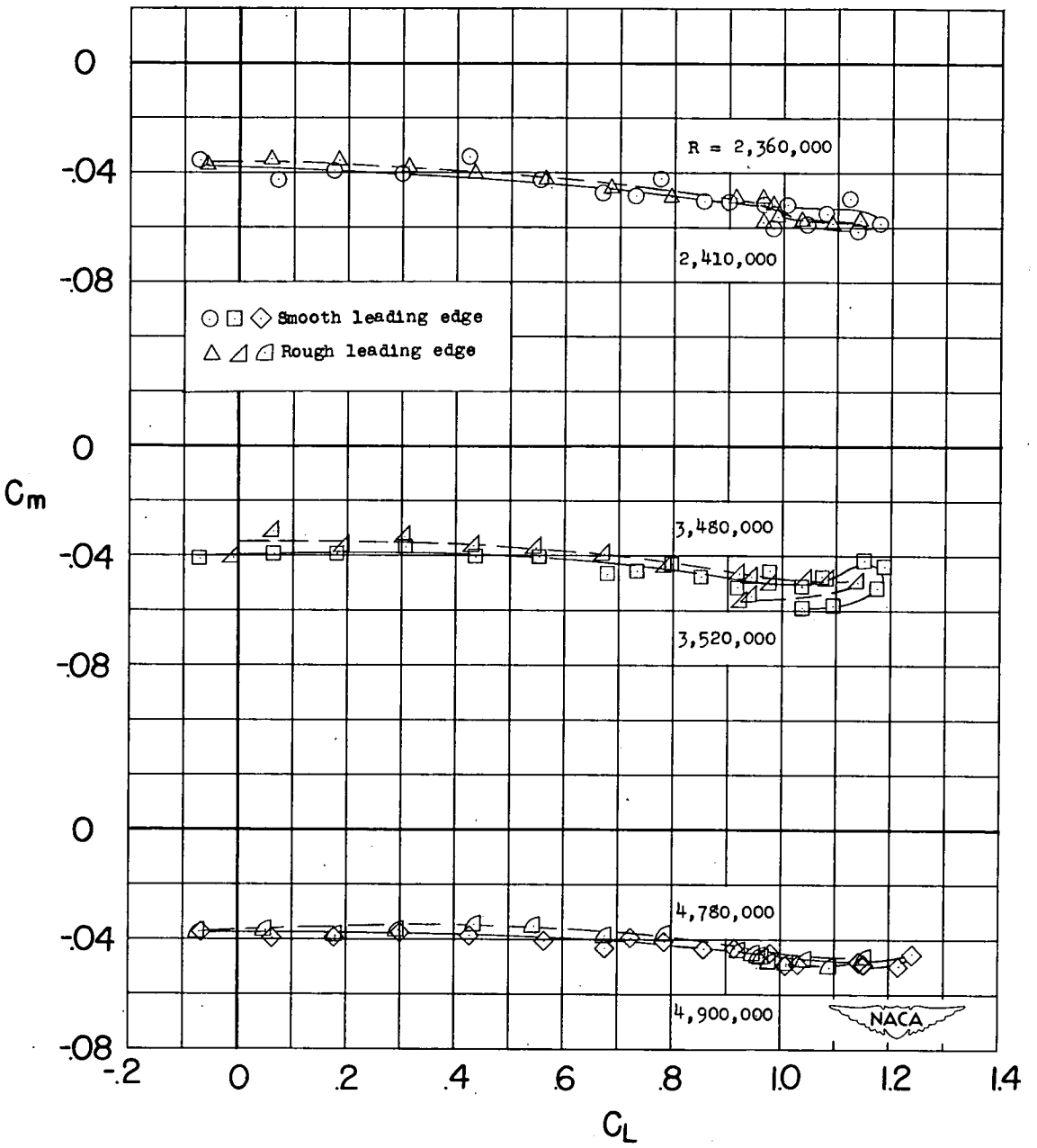

(b) Variation of C_m with C_L.

Figure 9.- Continued.

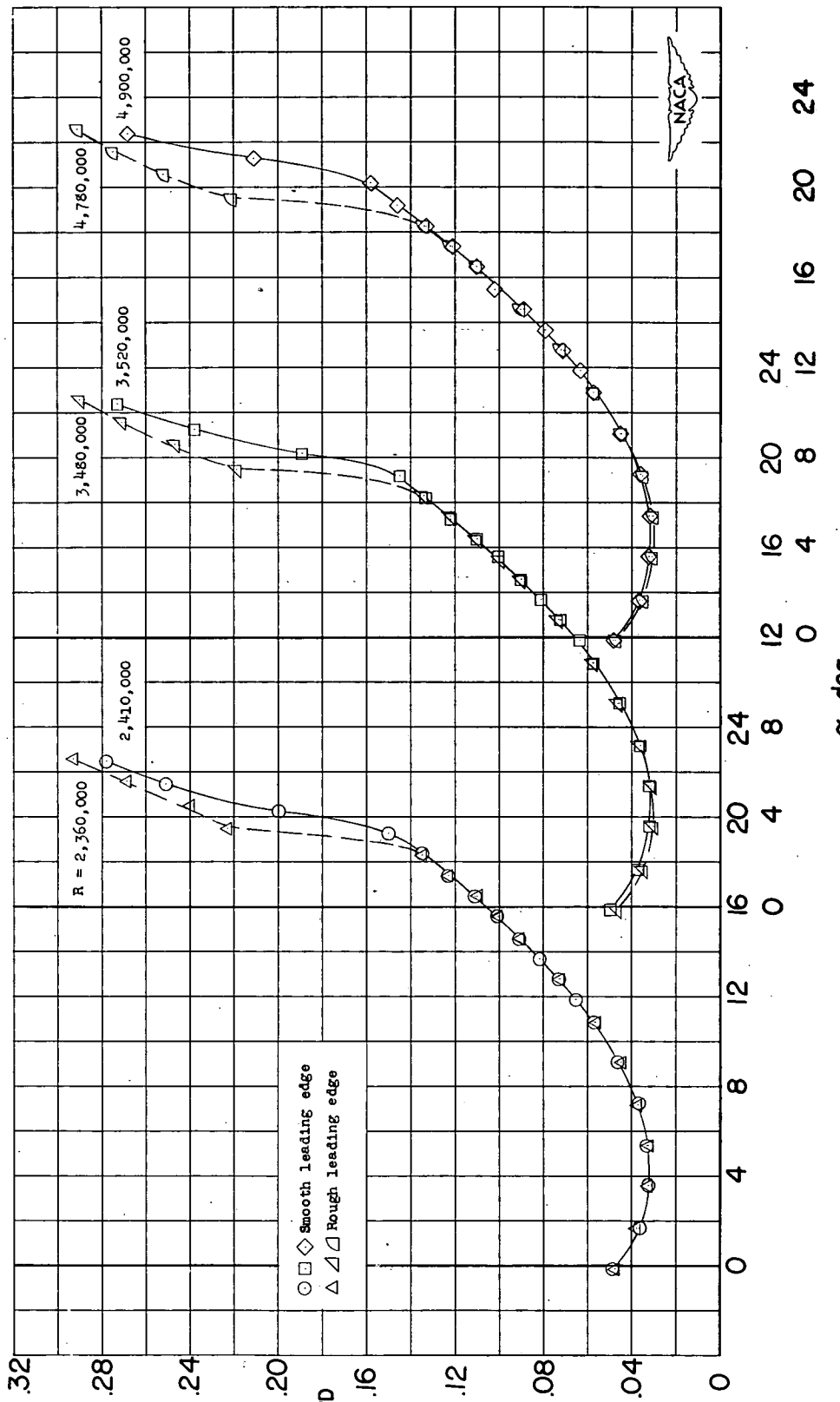

(c) Variation of C_D with α.

Figure 9.- Concluded.

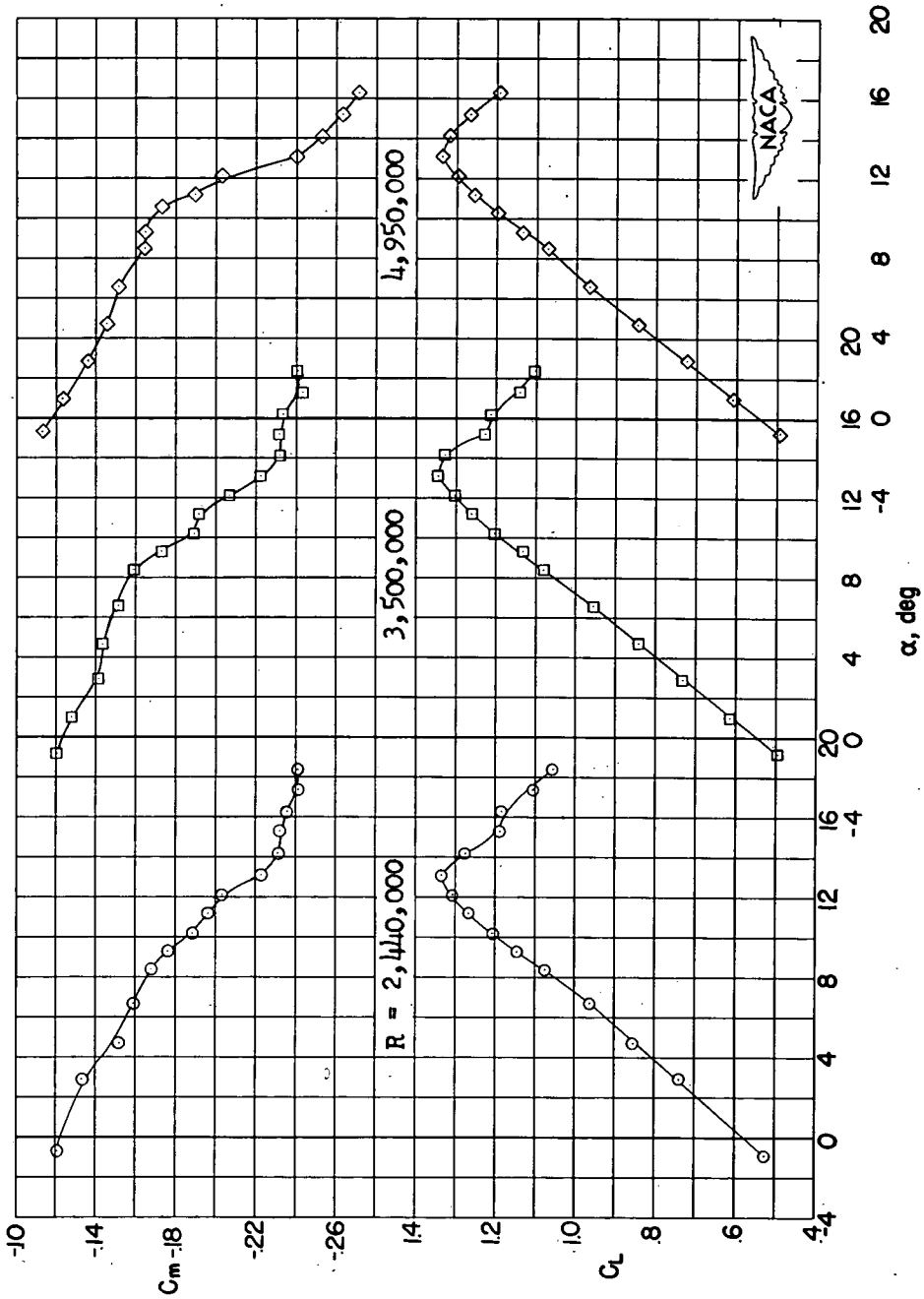

(a) Variation of C_L and C_m with α.

Figure 10.- Effect of Reynolds number on the aerodynamic characteristics of the wing with 35-percent-span leading-edge flaps. $\delta_f = 60°$.

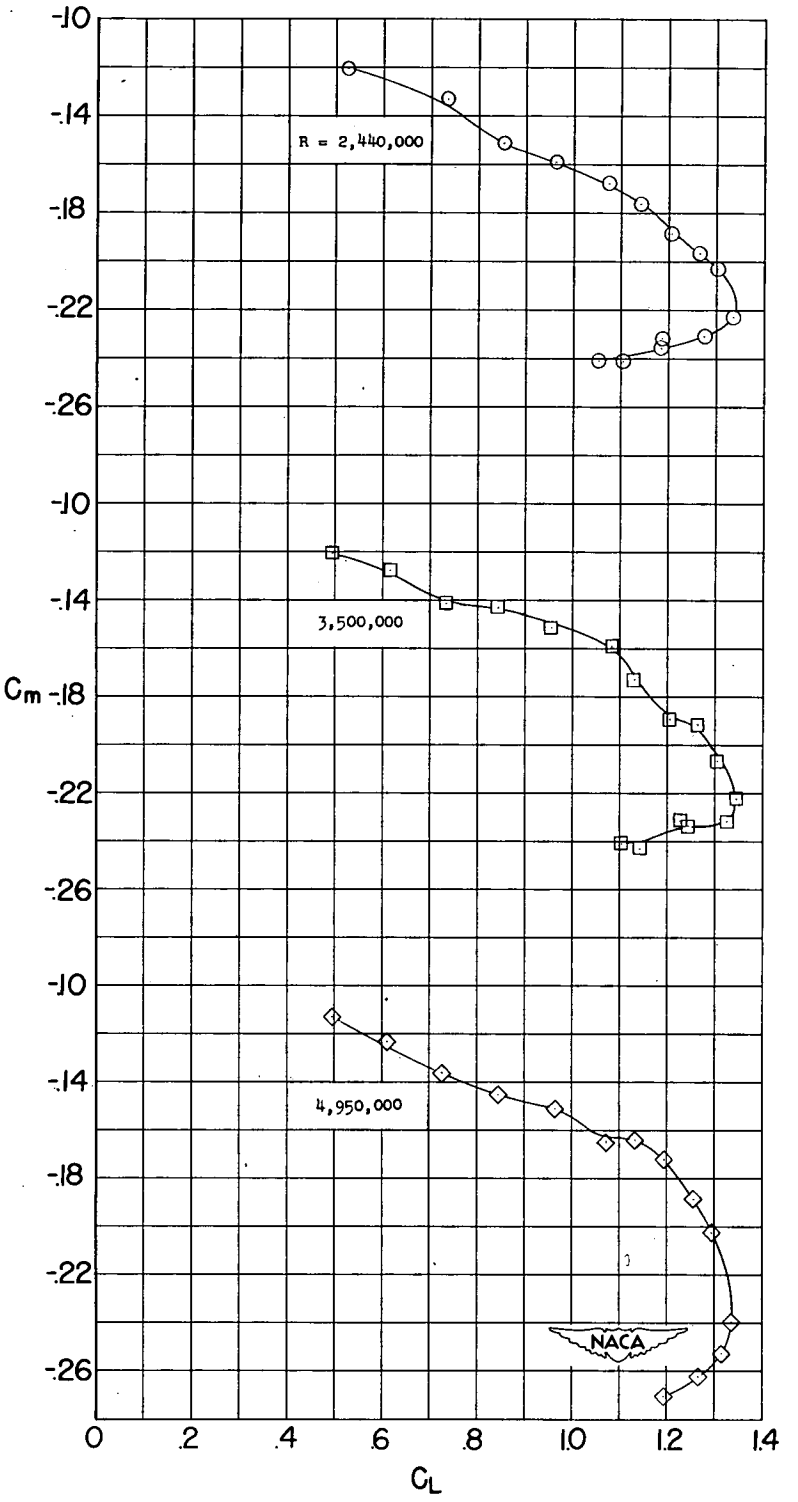

(b) Variation of C_m with C_L.

Figure 10.- Continued.

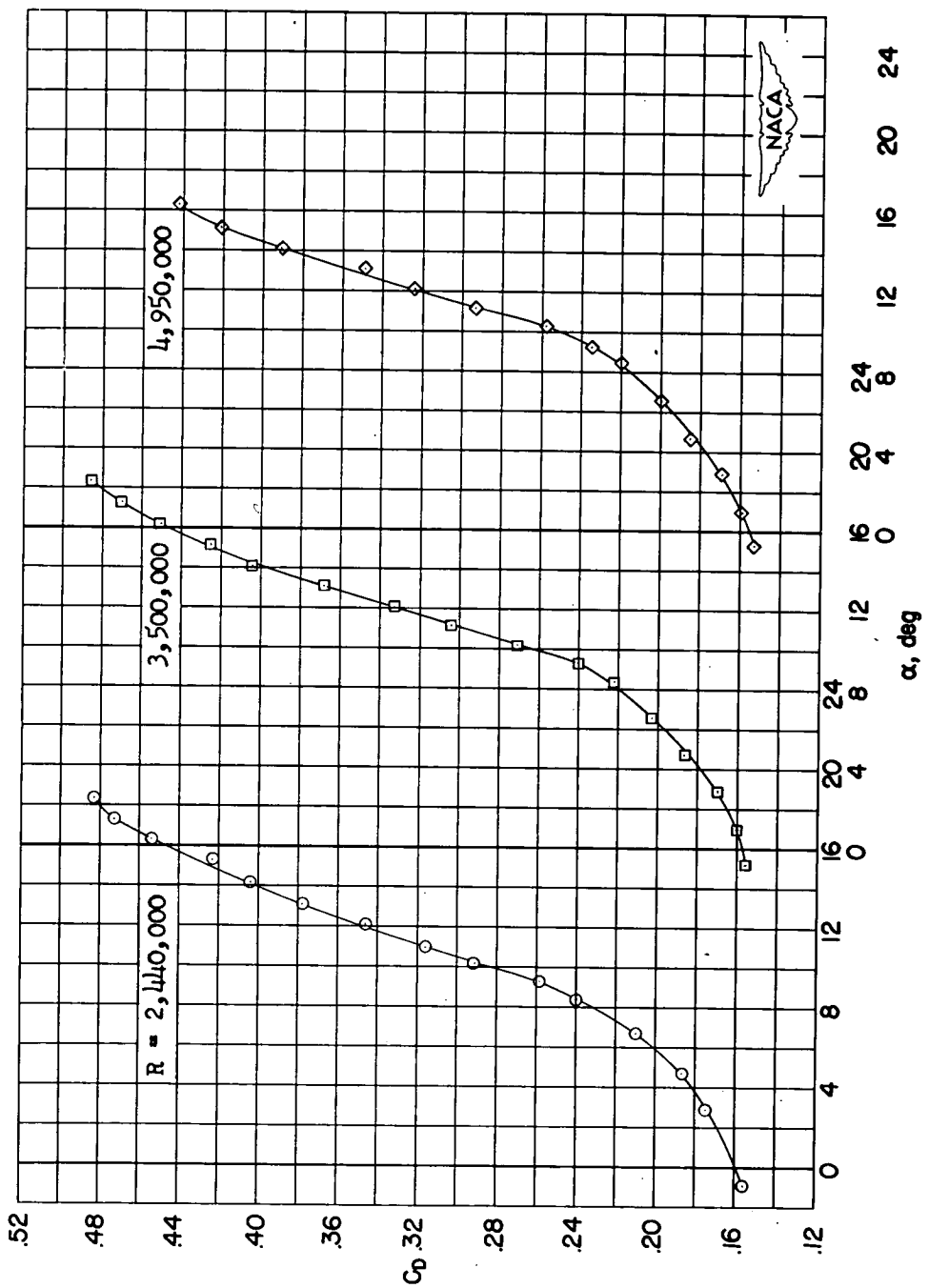

(c) Variation of C_D with α.

Figure 10.- Concluded.

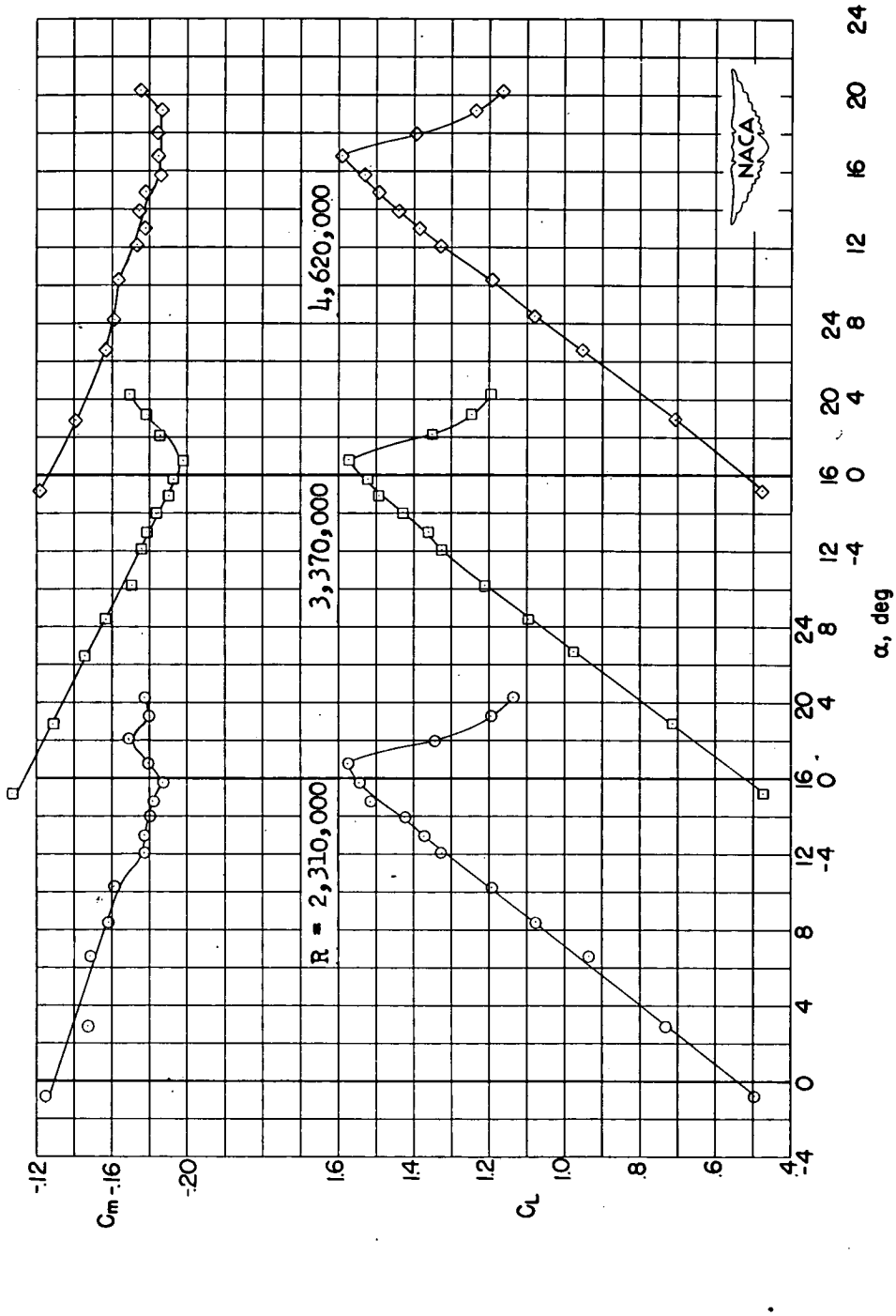

(a) Variation of C_L and C_m with α.

Figure 11.- Effect of Reynolds number on the aerodynamic characteristics of the wing with 70-percent-span leading-edge flaps. $\delta_f = 60°$.

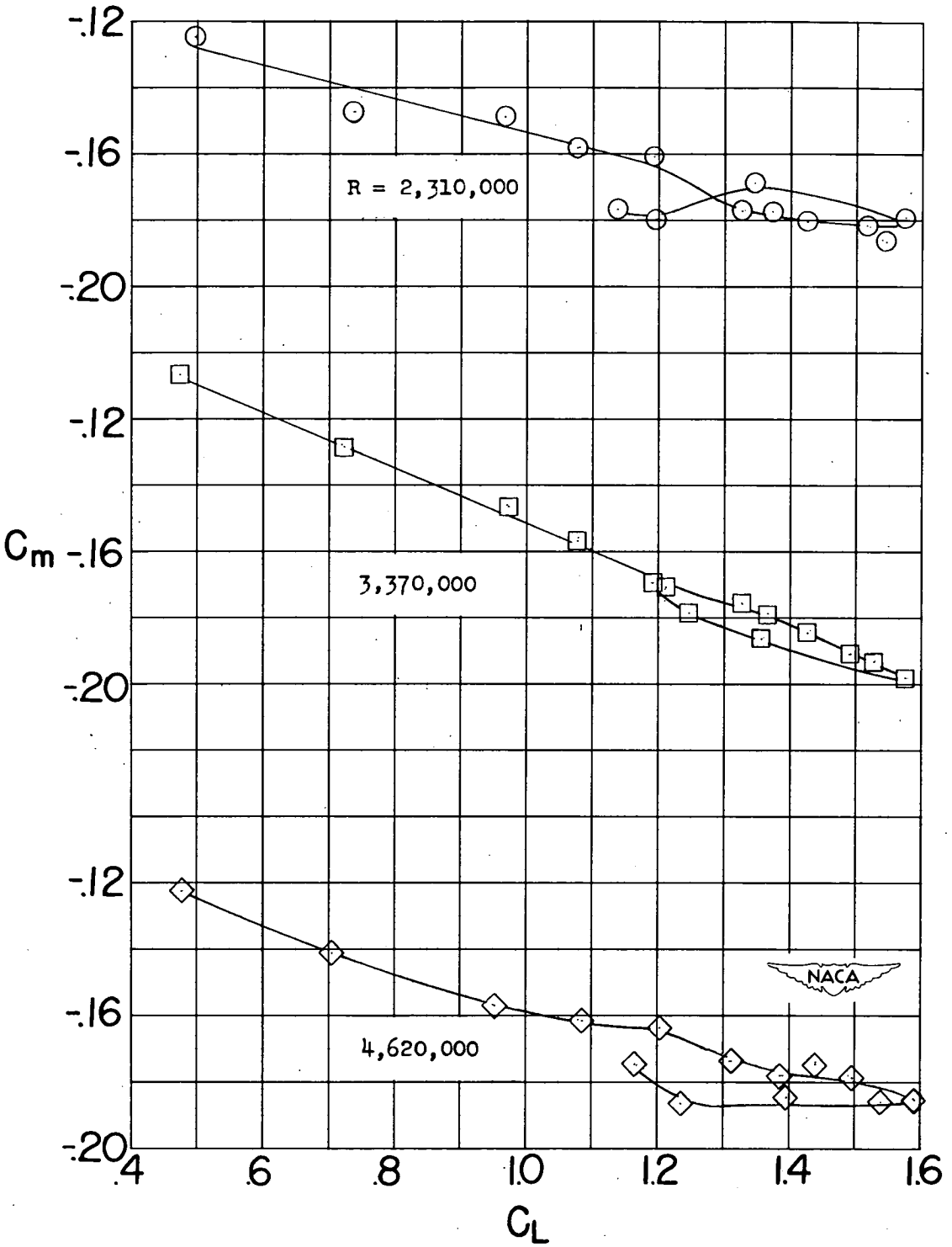

(b) Variation of C_m with C_L.

Figure 11.- Continued.

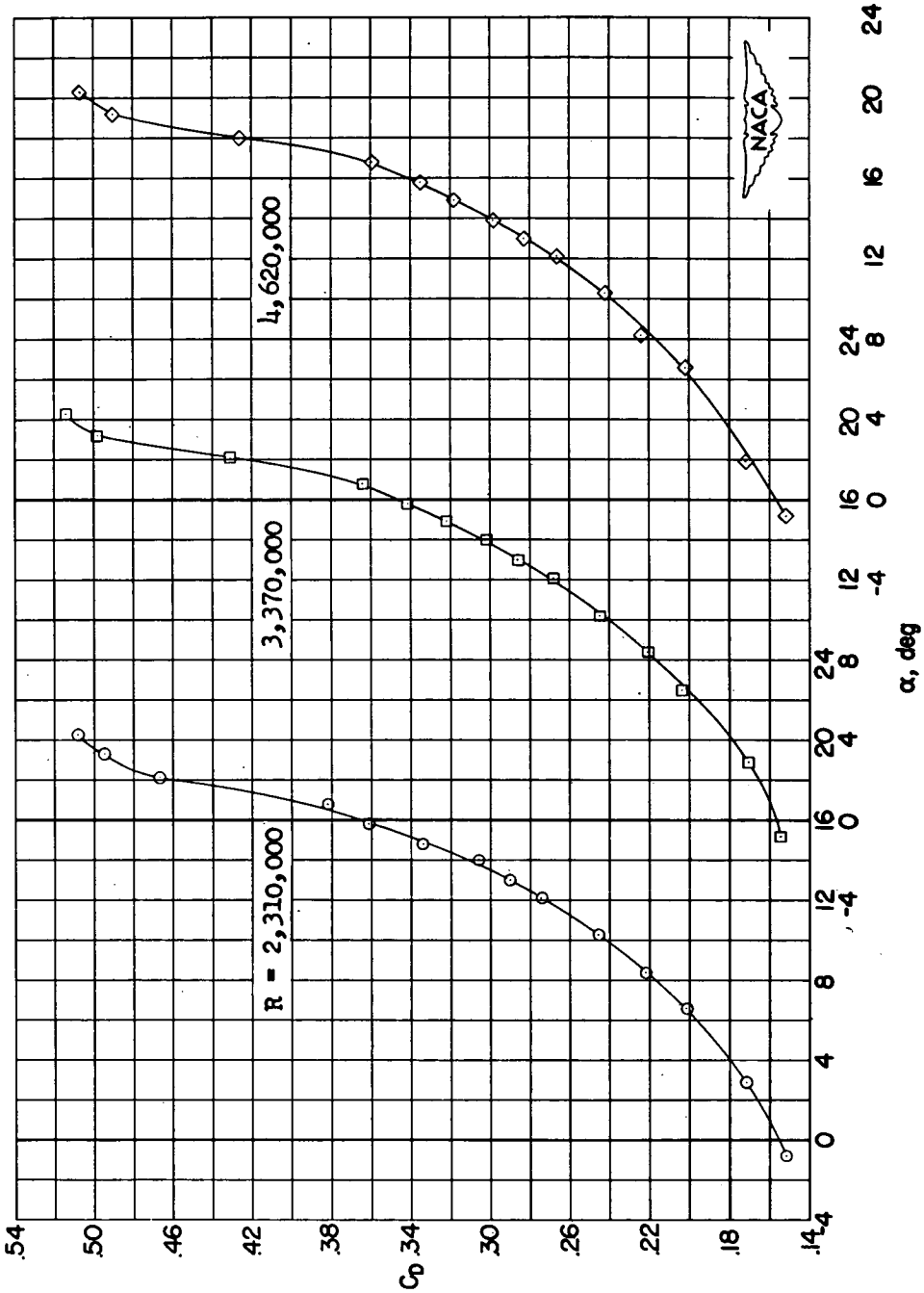

(c) Variation of C_D with α.

Figure 11.- Concluded.

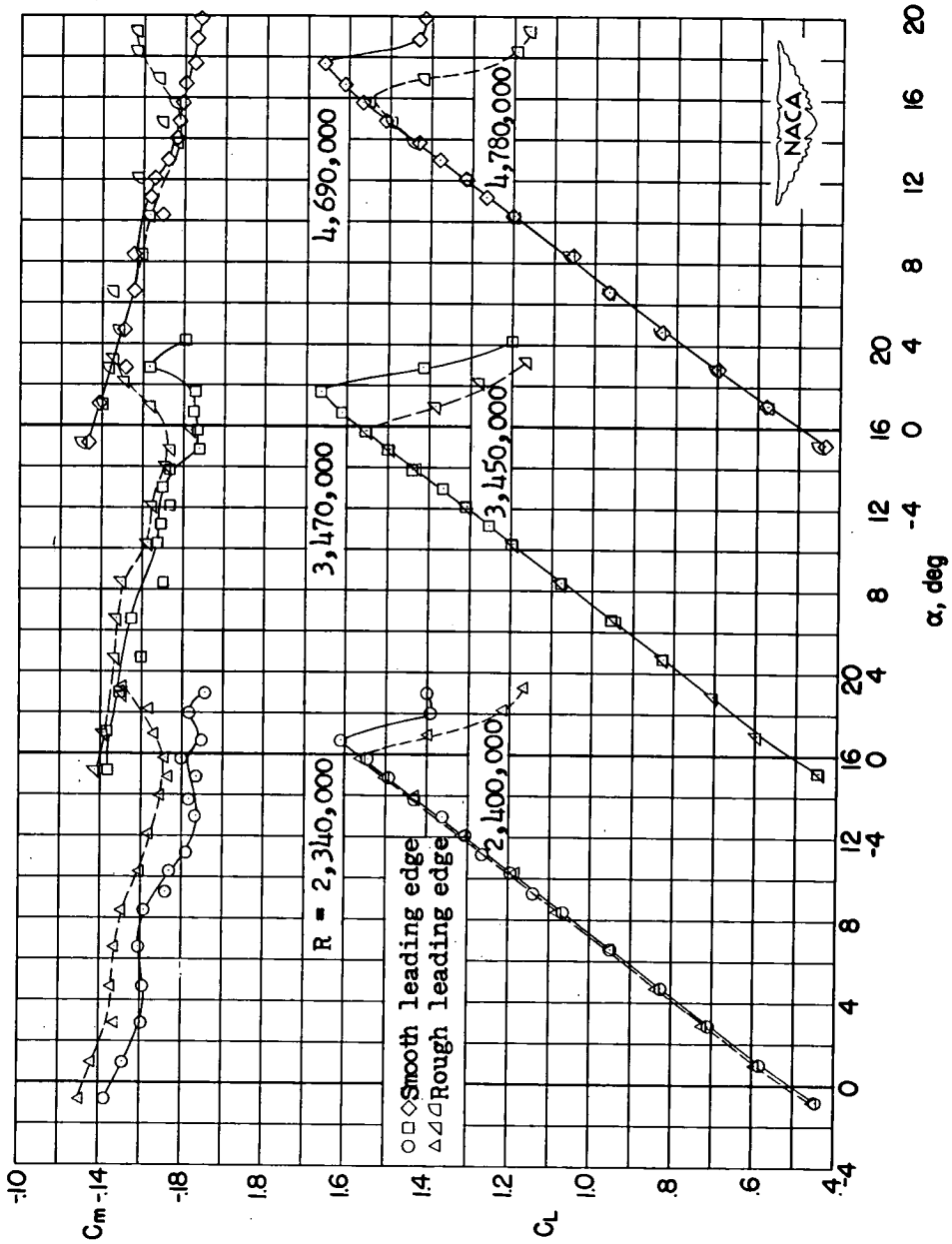

(a) Variation of C_L and C_m with α.

Figure 12.- Effect of Reynolds number and leading-edge roughness on the aerodynamic characteristics of the wing with full-span leading-edge flaps installed. $\delta_f = 60°$.

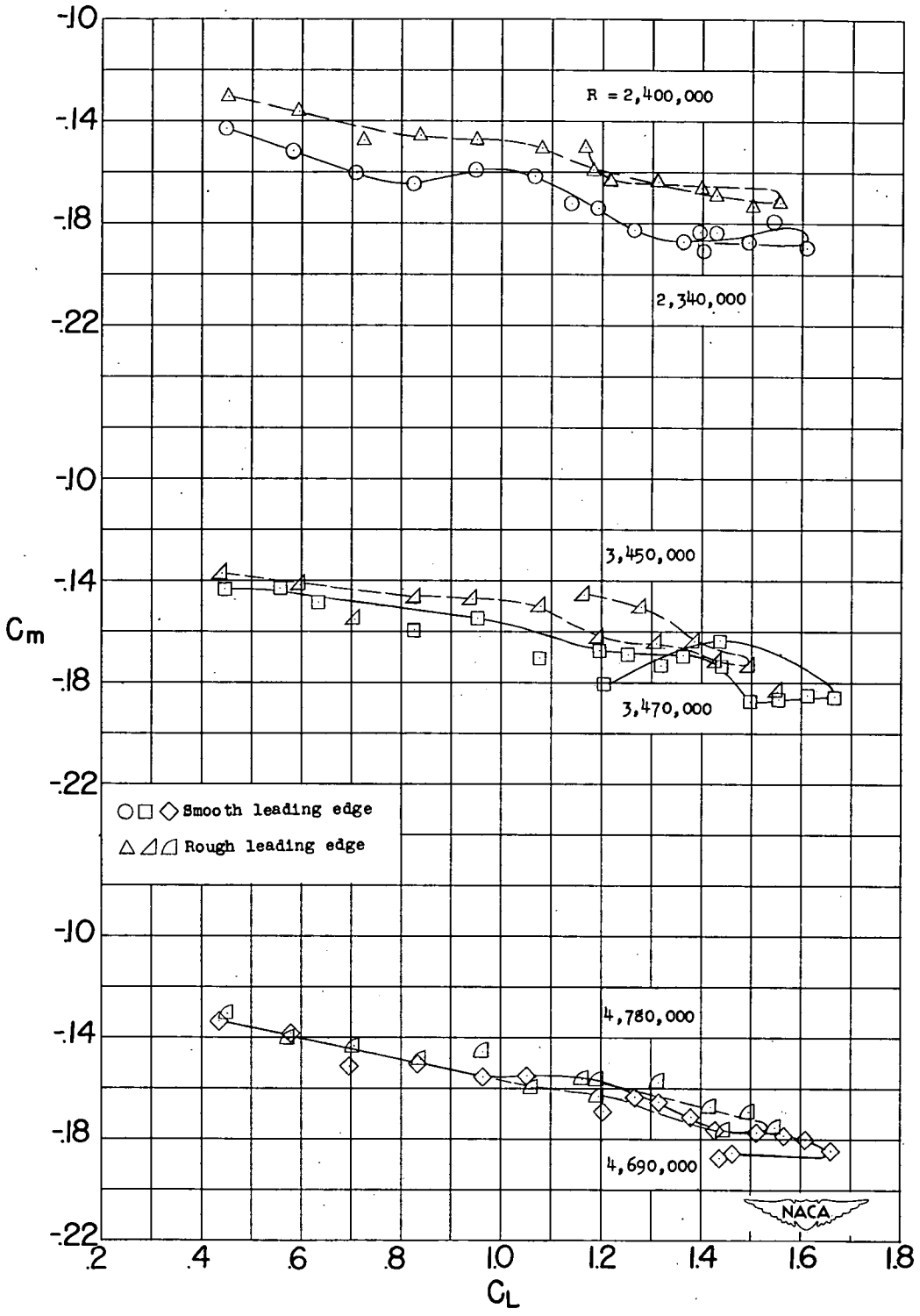

(b) Variation of C_m with C_L.

Figure 12.- Continued.

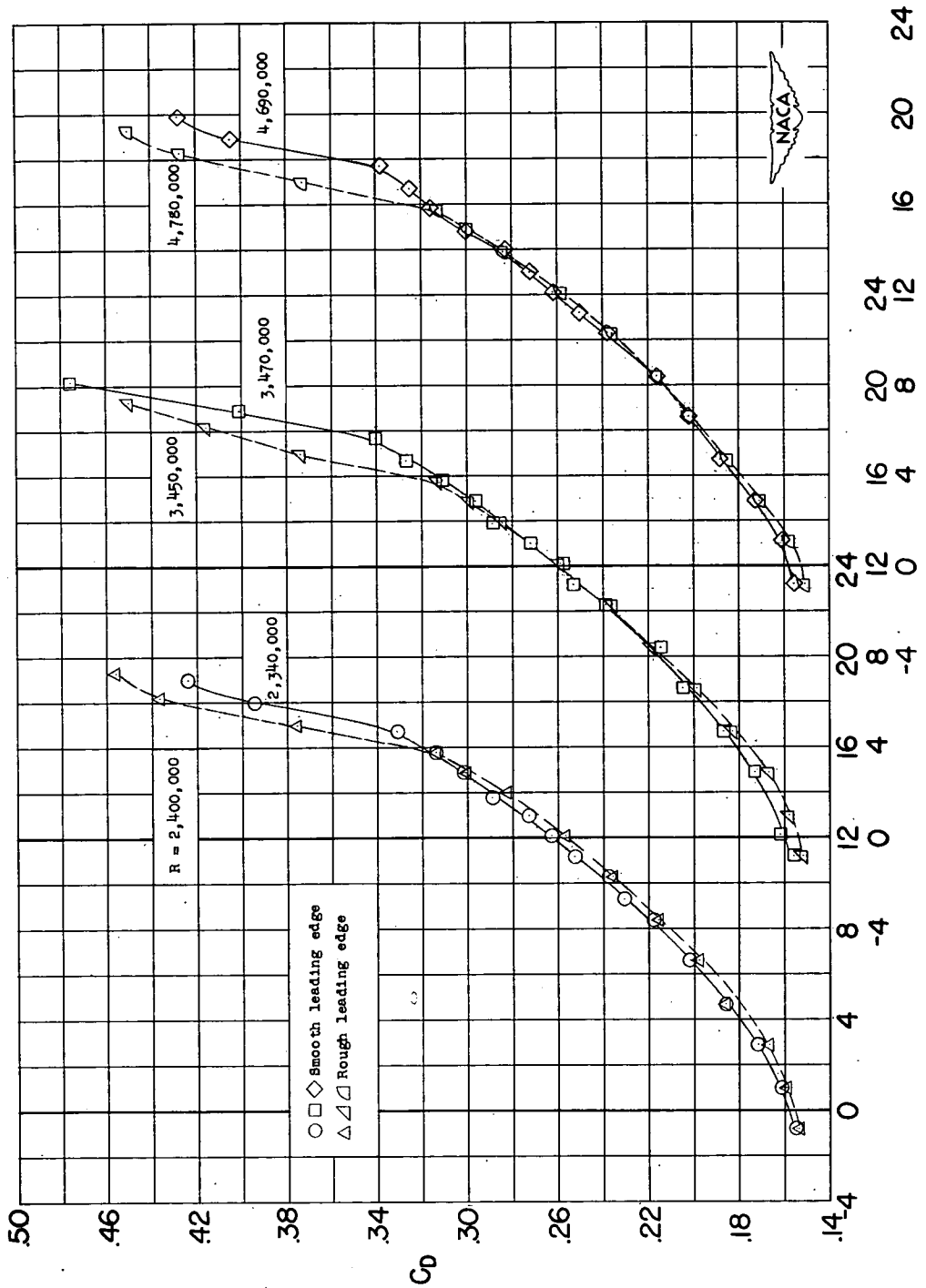

(c) Variation of C_D with α.

Figure 12.- Concluded.

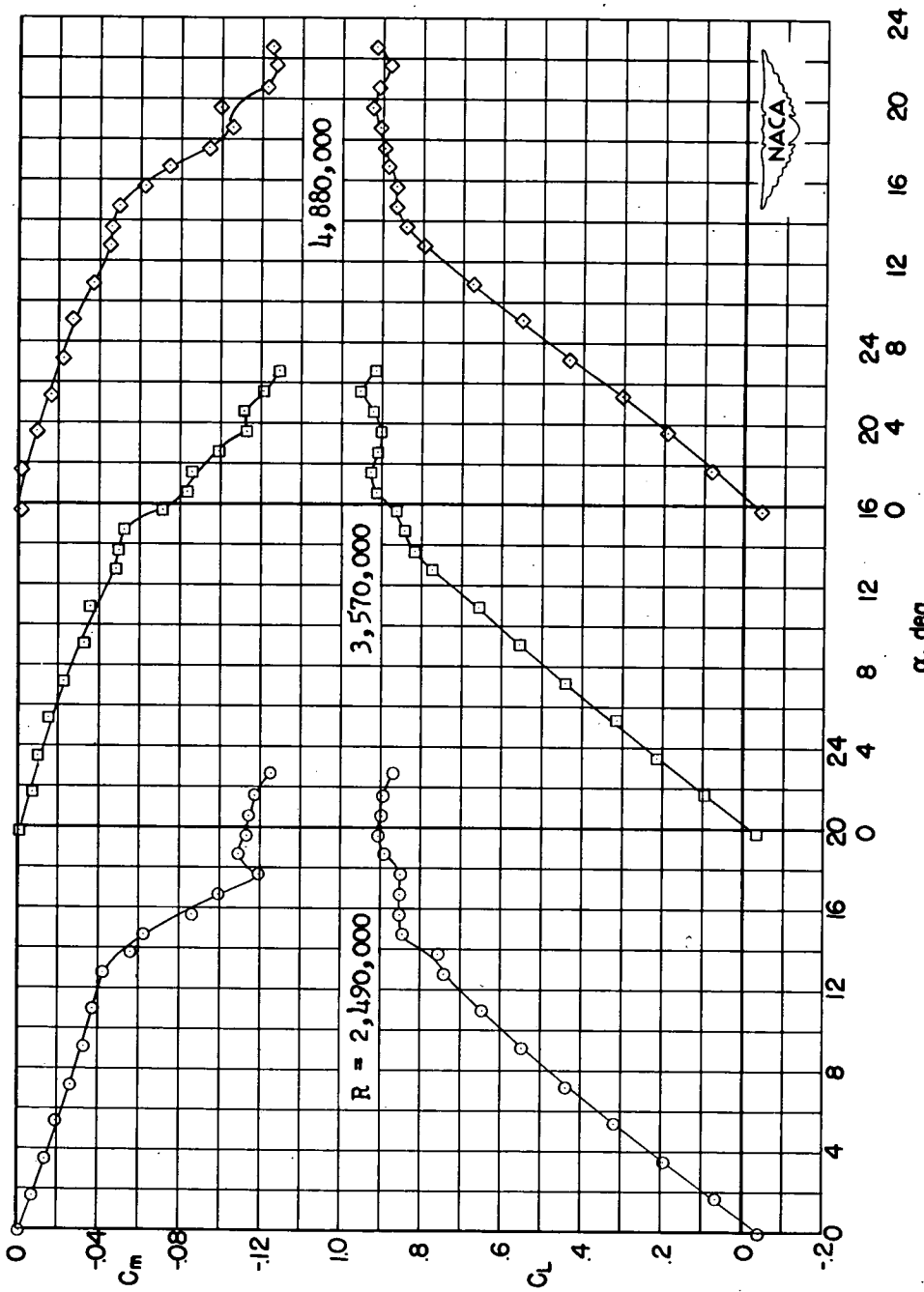

(a) Variation of C_L and C_m with α.

Figure 13.- Effect of Reynolds number on the aerodynamic characteristics of the wing with slat installed. $\delta_f = 0^\circ$.

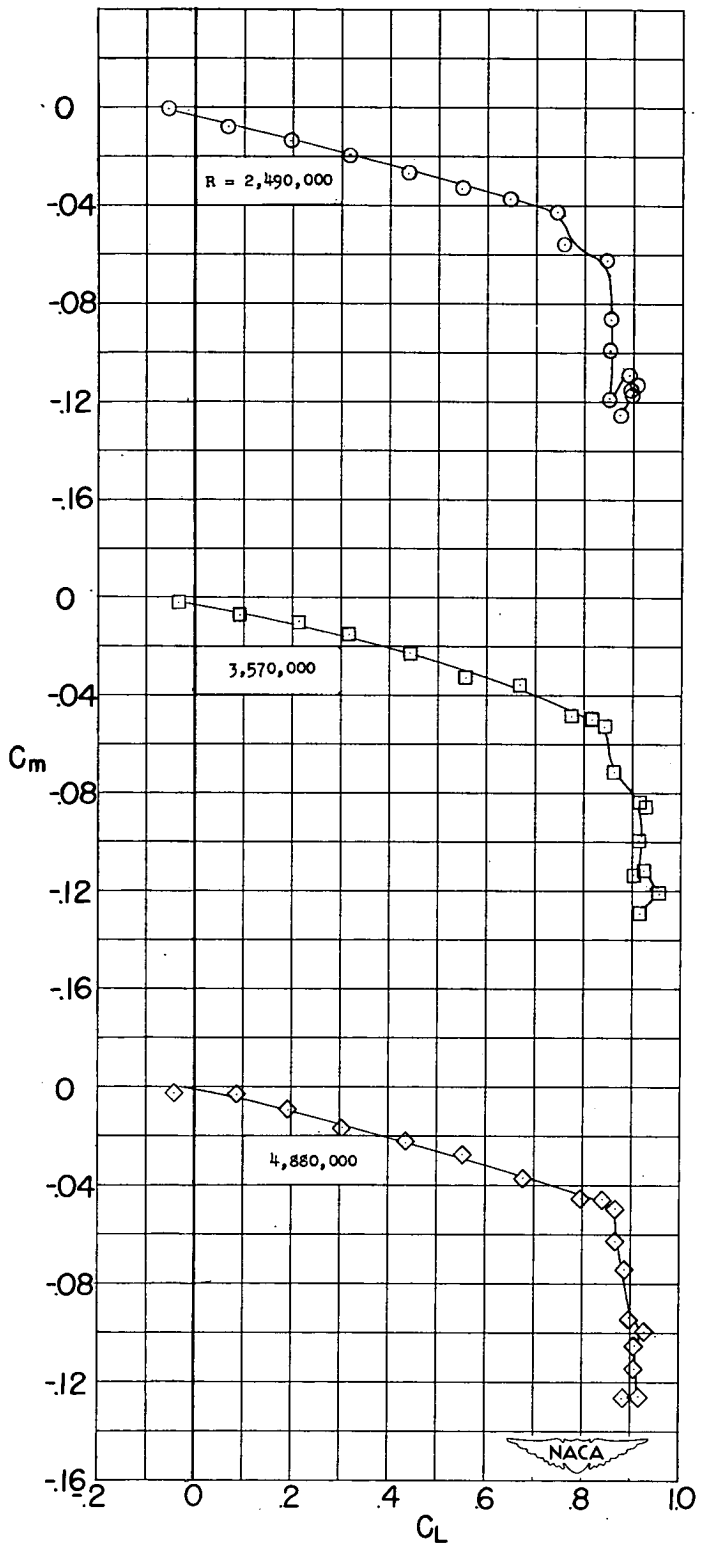

(b) Variation of C_m with C_L.

Figure 13.- Continued.

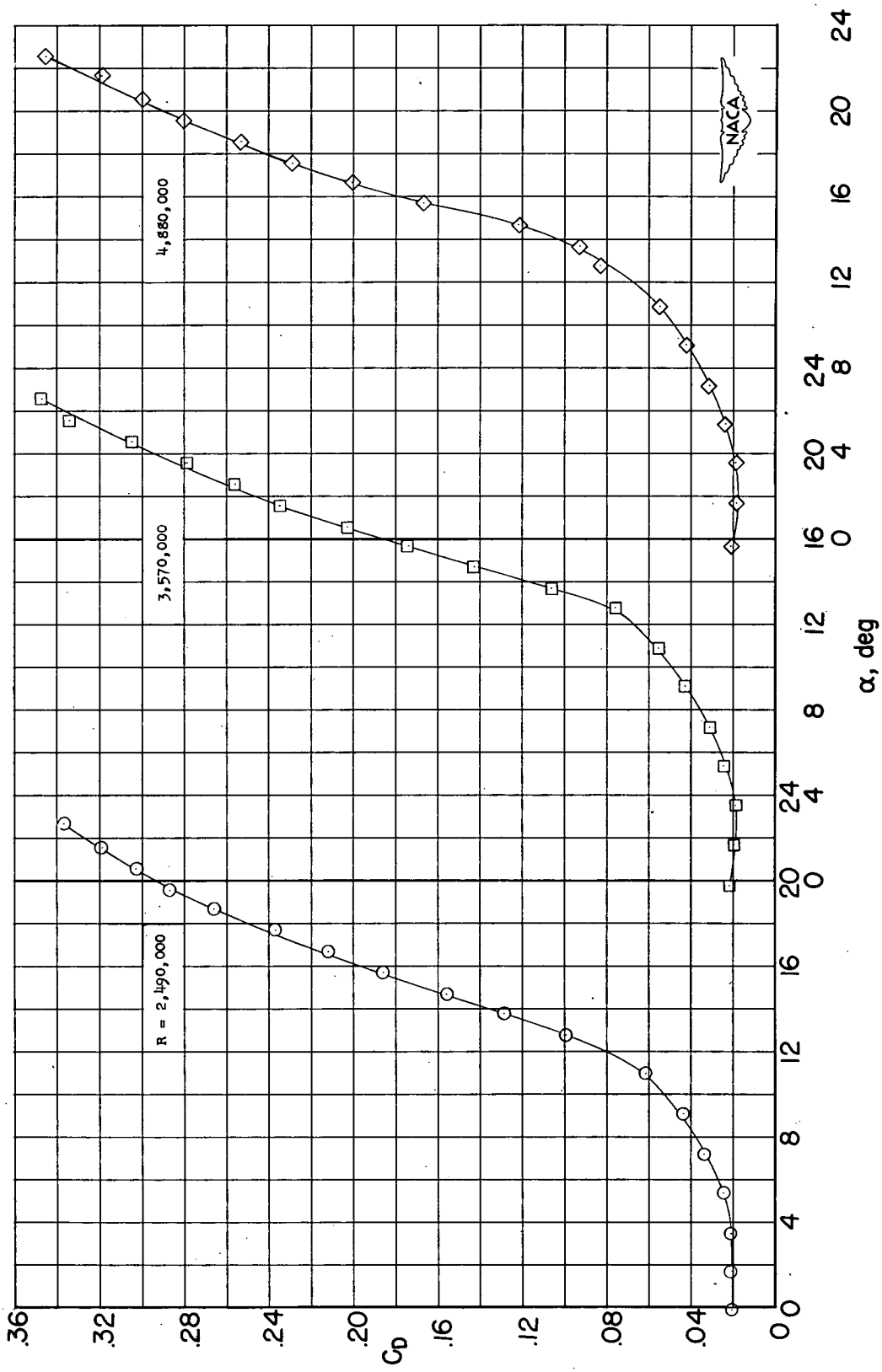

(c) Variation of C_D with α.

Figure 13.- Concluded.

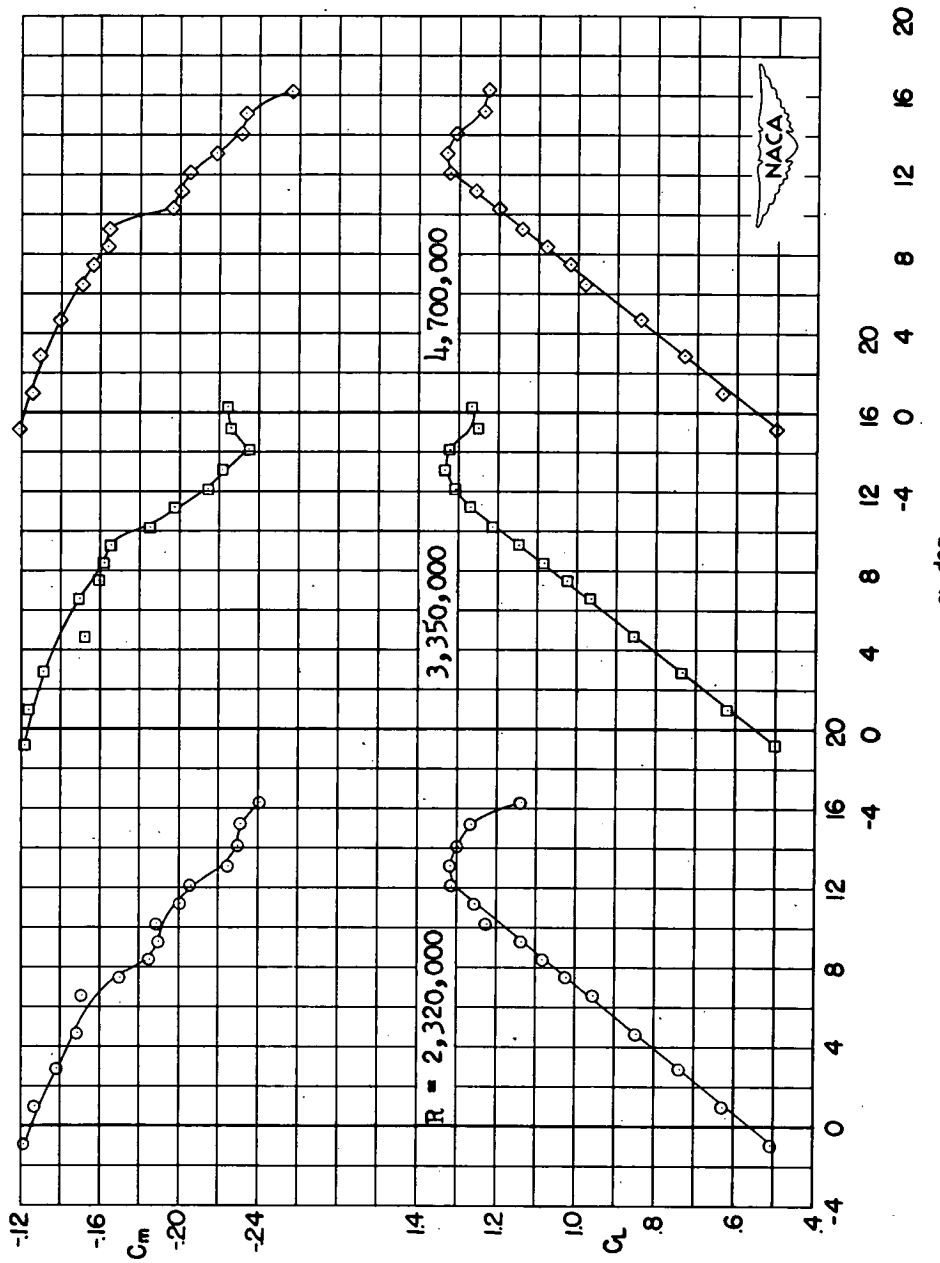

(a) Variation of C_L and C_m with α.

Figure 14.- Effect of Reynolds number on the aerodynamic characteristics of the wing with slat installed $\delta_f = 60°$.

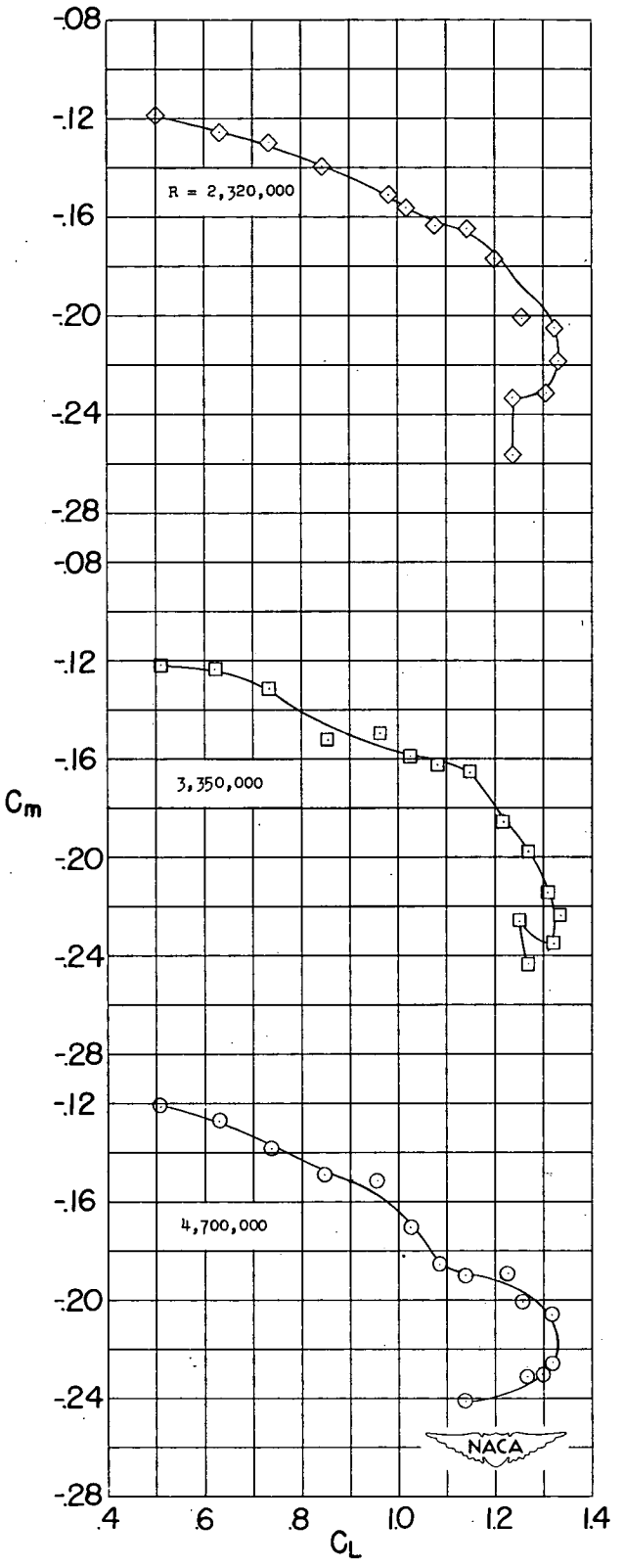

(b) Variation of C_m with C_L.

Figure 14.- Continued.

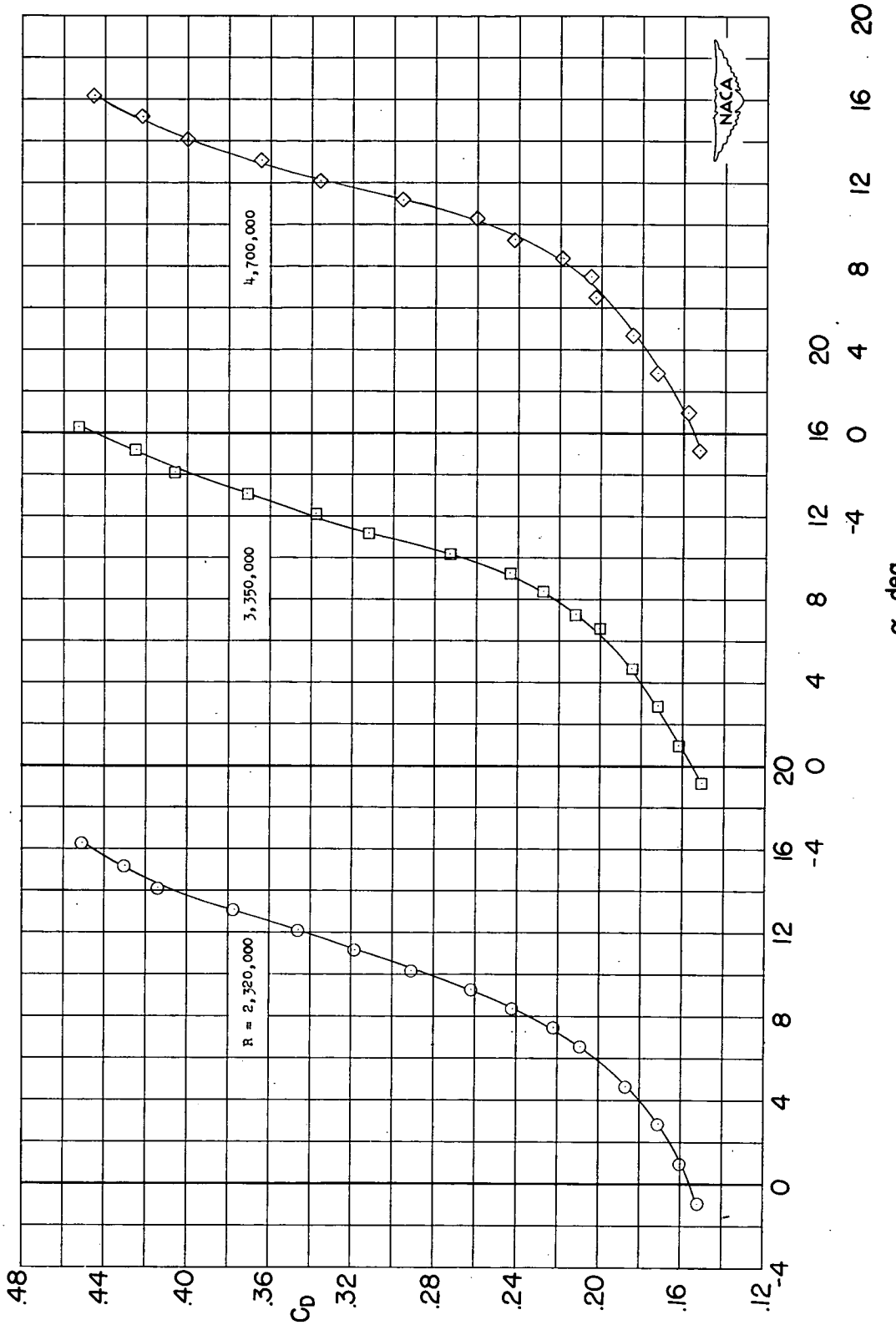

(c) Variation of C_D with α.

Figure 14.- Concluded.

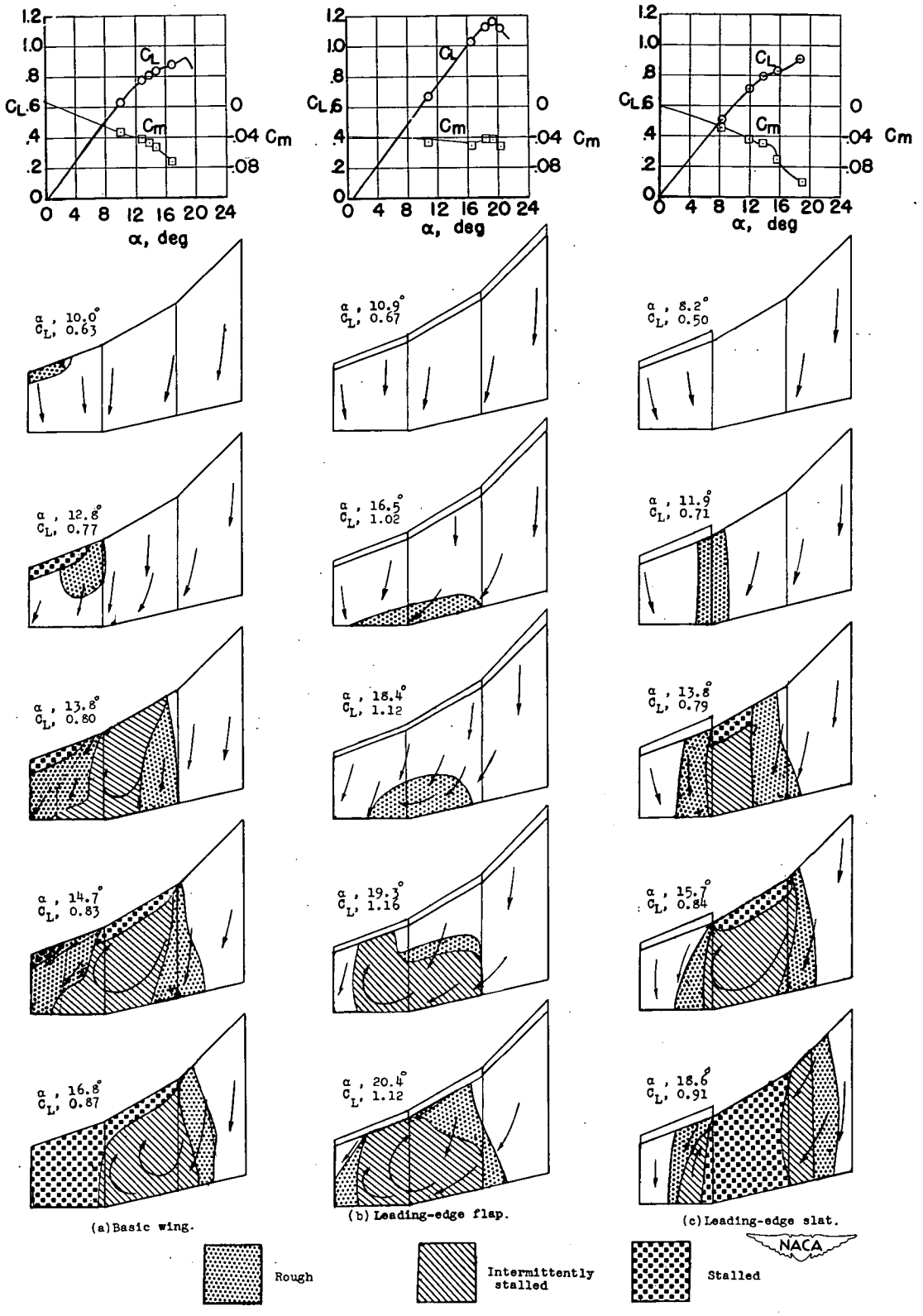

Figure 15.- Stall diagrams of wing with several high-lift devices installed. Arrows indicate direction of flow; $\delta_f = 0^o$; $R \approx 3.5 \times 10^6$.

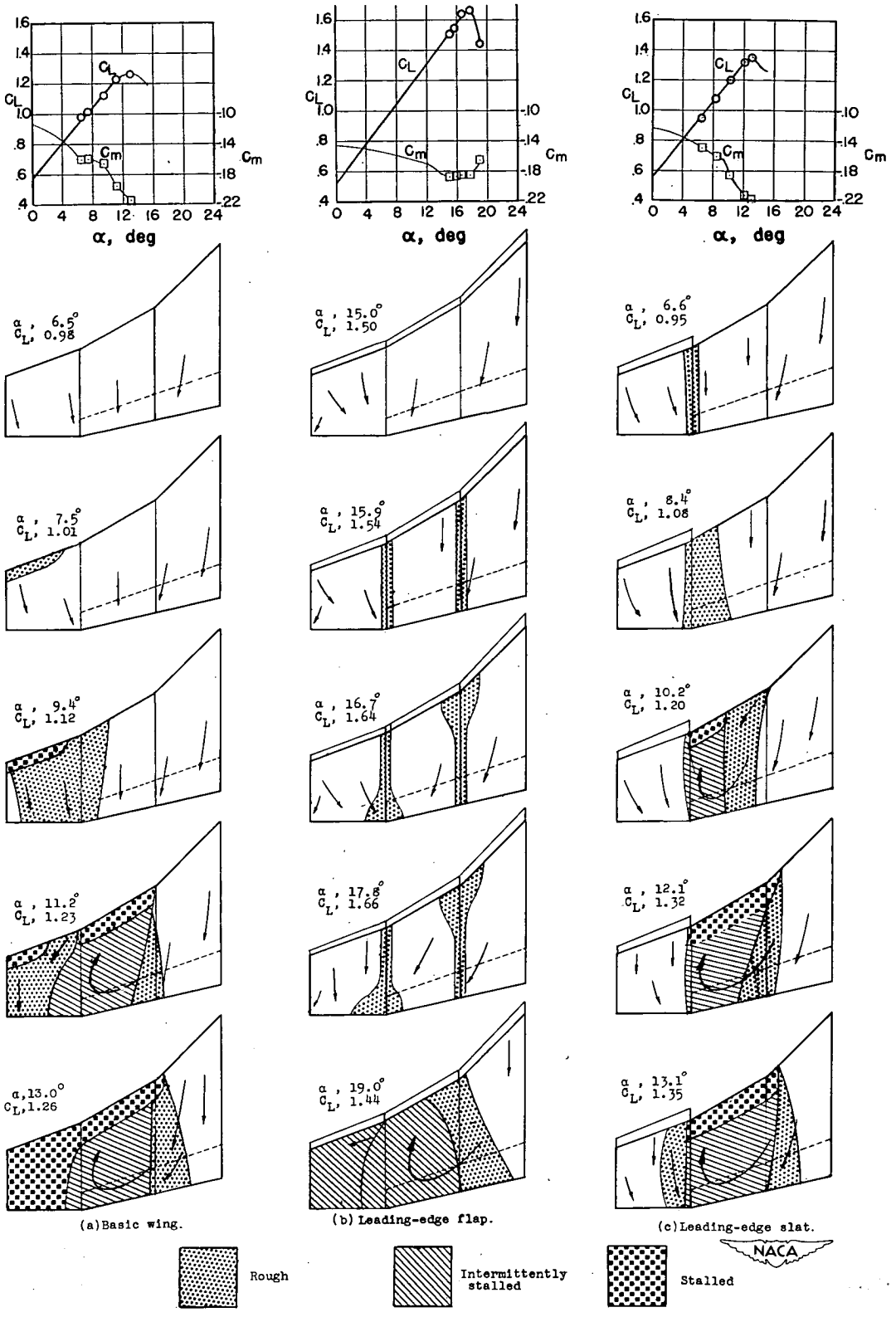

Figure 16.- Stall diagrams of wing with several high-lift devices installed. Arrows indicate direction of flow; $\delta_f = 60^\circ$; $R \approx 3.5 \times 10^6$.

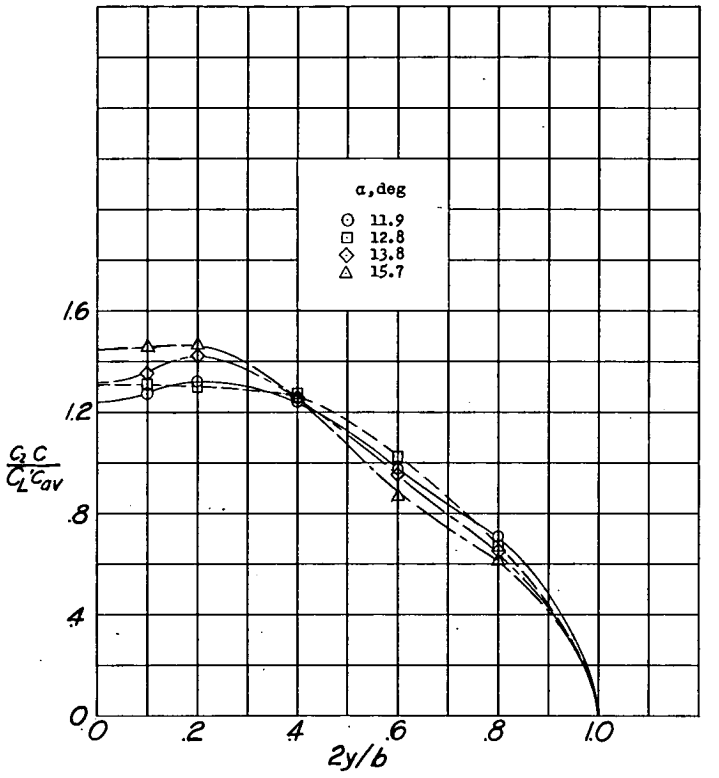

(a) Span load distributions.

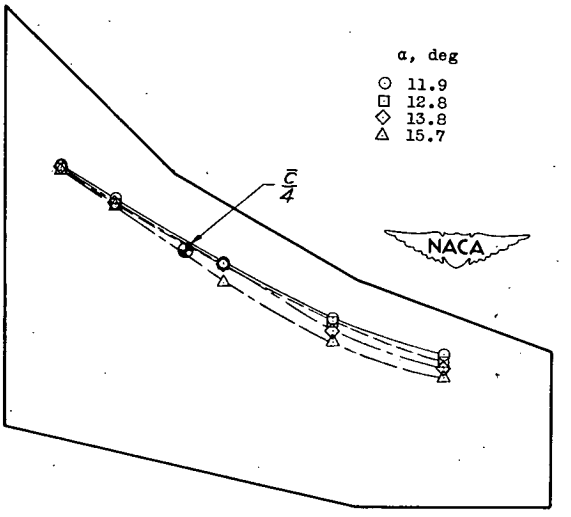

(b) Location of local center of pressure.

Figure 17.- Typical results from pressure-distribution measurements over basic wing. $R \approx 3.5 \times 10^6$.

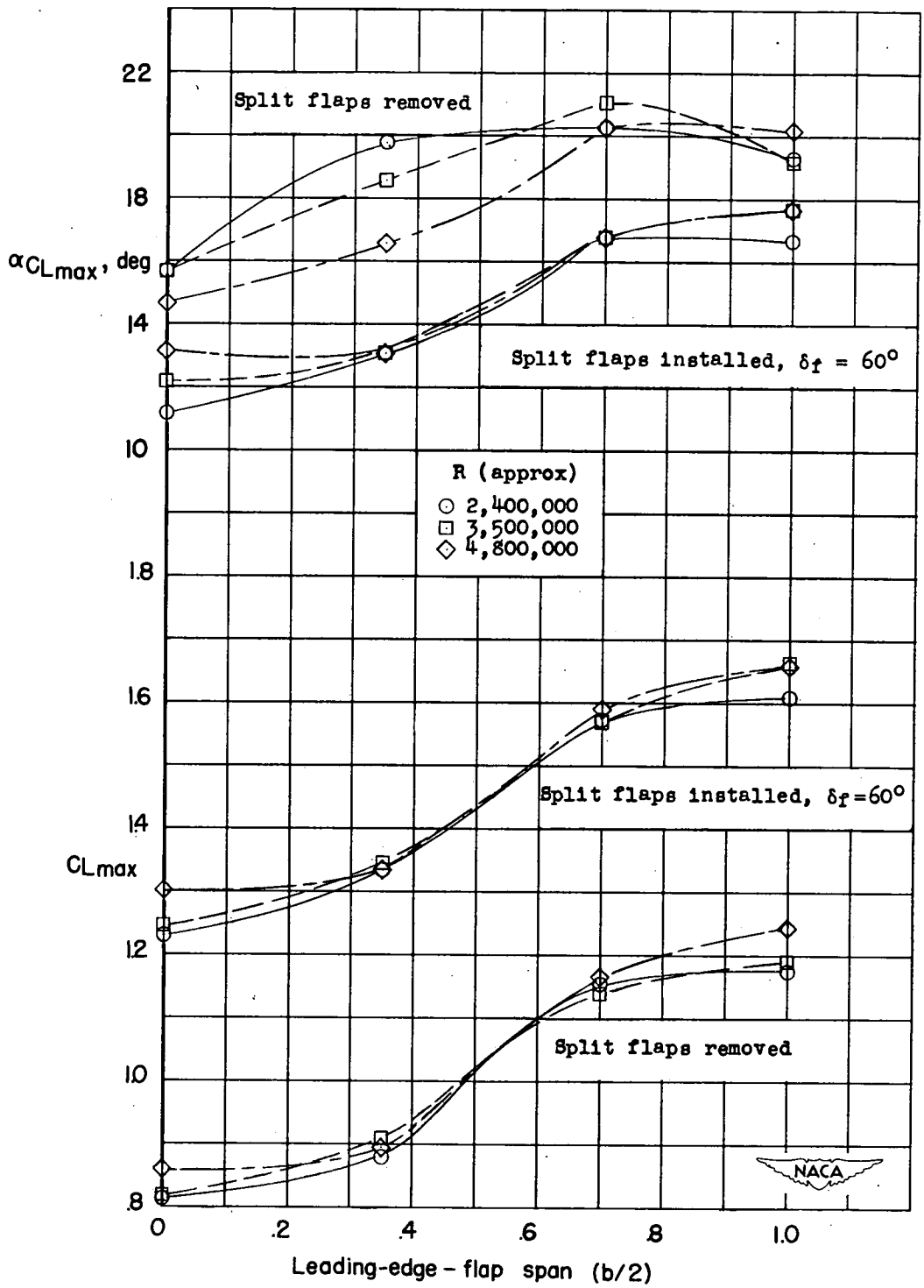

(a) Maximum lift.

Figure 18.- Summary of effects of varying the leading-edge-flap span.

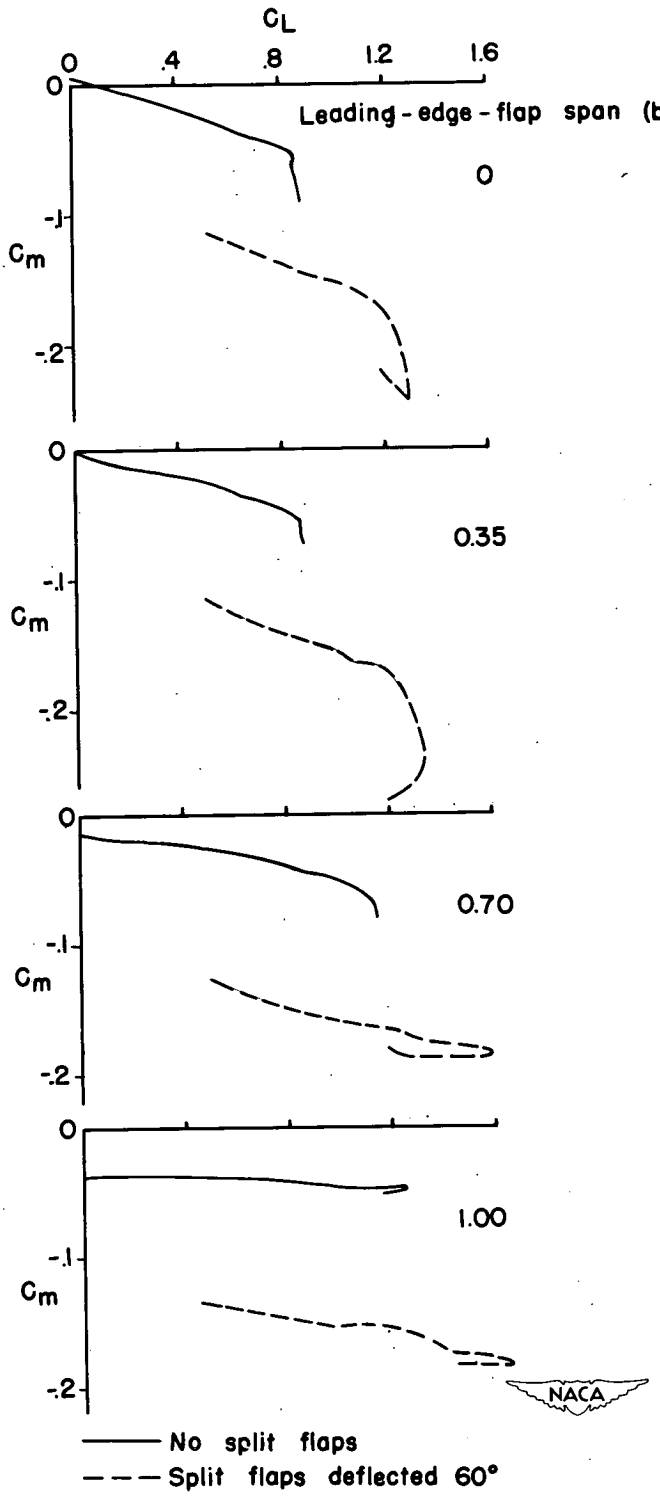

(b) Pitching moment. $R \approx 4.8 \times 10^6$.

Figure 18.- Concluded.

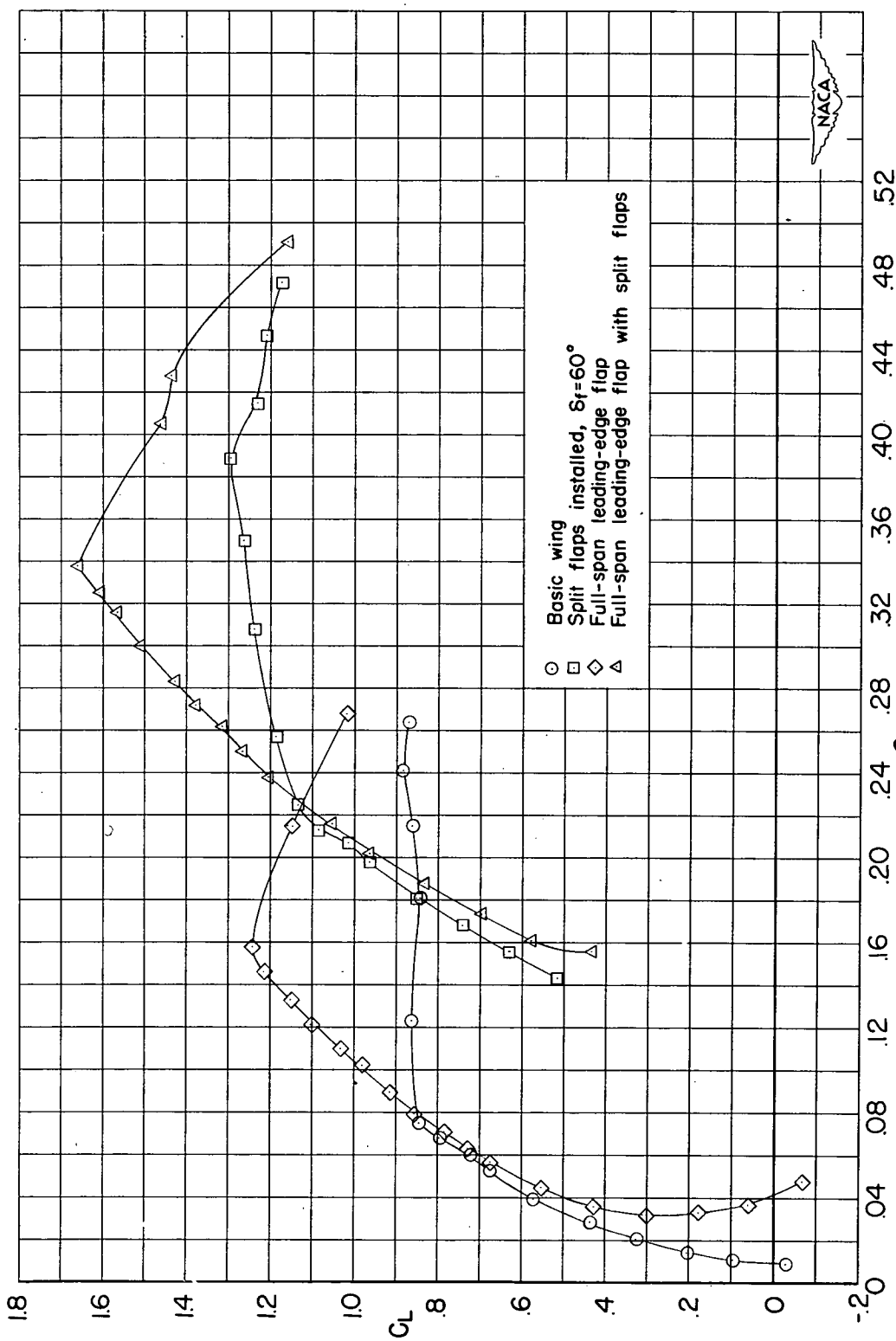

Figure 19.- Effect of high-lift devices on the variation of C_L with C_D. $R \approx 4.8 \times 10^6$.

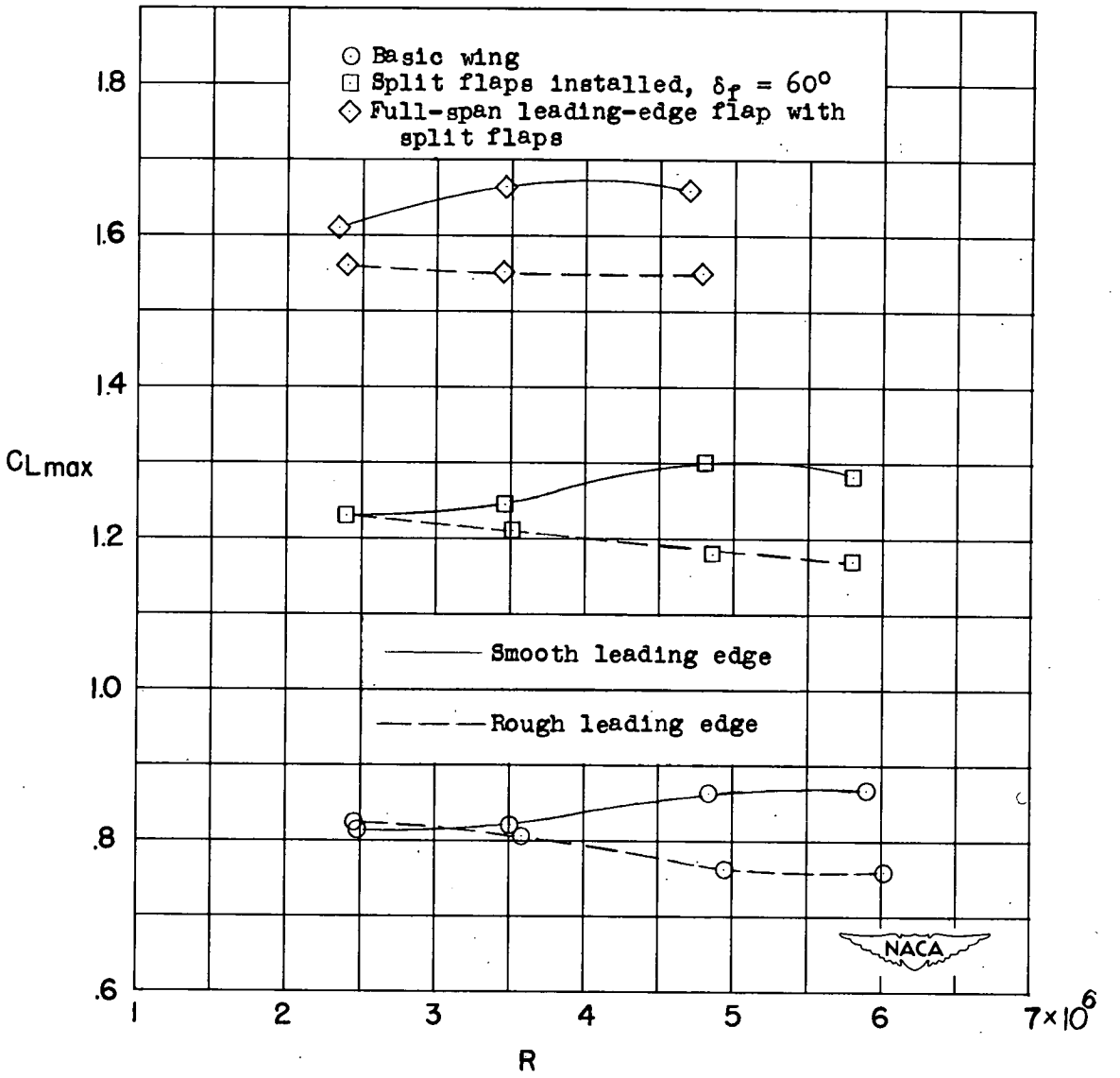

Figure 20.- Summary of maximum lift coefficients as affected by Reynolds number.